



A comparison of time series similarity measures for classification and change detection of ecosystem dynamics

S. Lhermitte ^{a,b,*}, J. Verbesselt ^c, W.W. Verstraeten ^{b,d}, P. Coppin ^e

^a Centro de Estudios Avanzados en Zonas Aridas (CEAZA), Universidad de la Serena, La Serena, Chile

^b Royal Netherlands Meteorological Institute (KNMI), De Bilt, The Netherlands

^c Wageningen University, Centre for Geo-Information, Wageningen, The Netherlands

^d Eindhoven University of Technology, Applied Physics, Eindhoven, The Netherlands

^e M3-BIORES, Biosystems Department, Katholieke Universiteit Leuven, Leuven, Belgium

ARTICLE INFO

Article history:

Received 26 September 2009

Received in revised form 18 March 2011

Accepted 25 June 2011

Available online 27 August 2011

Keywords:

Time series analysis

Ecosystem dynamics

Classification

Change detection

ABSTRACT

Time series of remote sensing imagery or derived vegetation indices and biophysical products have been shown particularly useful to characterize land ecosystem dynamics. Various methods have been developed based on temporal trajectory analysis to characterize, classify and detect changes in ecosystem dynamics. Although time series similarity measures play an important role in these methods, a quantitative comparison of the similarity measures is lacking. The objective of this study was to provide an overview and quantitative comparison of the similarity measures in function of varying time series and ecosystem characteristics, such as amplitude, timing and noise effects. For this purpose, the performance was evaluated for the commonly used similarity measures (D), ranging from Manhattan (D_{Man}), Euclidean (D_E) and Mahalanobis (D_{Mah}) distance measures, to correlation (D_{CC}), Principal Component Analysis (PCA; D_{PCA}) and Fourier based (D_{FFT} , D_E , D_{FK}) similarities. The quantitative comparison consists of a series of Monte-Carlo simulations based on subsets of global MODIS Normalized Difference Vegetation index (NDVI) and Enhanced Vegetation Index (EVI) and Leaf Area Index (LAI) data. Results of the simulations reveal four main groups of time series similarity measures with different sensitivities: (i) D_{Man} , D_E , D_{PCA} , D_{FK} quantify the difference in time series values, (ii) D_{Mah} accounts for temporal correlation and non-stationarity of variance, (iii) D_{CC} measures the temporal correlation, and (iv) the Fourier based D_{FFT} and D_E show their specific sensitivity based on the selected Fourier components. The difference measures show relatively the highest sensitivity to amplitude effects, whereas the correlation based measures are highly sensitive to variations in timing and noise. The Fourier based measures, finally, depend highly on the signal to noise ratio and the balance between amplitude and phase dominance. The heterogeneity in sensitivity of each D stresses the importance of (i) understanding the time series characteristics before applying any classification of change detection approach and (ii) defining the variability one wants to identify/account for. This requires an understanding of the ecosystem dynamics and time series characteristics related to the baseline, amplitude, timing, noise and variability of the ecosystem time series. This is also illustrated in the quantitative comparison, where the different sensitivities of D for the NDVI, EVI, and LAI data relate specifically to the temporal characteristics of each data set. Additionally, the effect of noise and intra- and interclass variability is demonstrated in a case study based on land cover classification.

© 2011 Elsevier Inc. All rights reserved.

1. Introduction

Assessing and monitoring the state of ecosystems are key requirements for global change research (Fischlin et al., 2007), biodiversity conservation and ecosystem management (Coops et al., 2009; Turner et al., 2007). Satellite remote sensing has long been used as a tool to assess land ecosystem dynamics as they provide consistent measurements at a spatio-temporal scale which is appropriate for

capturing bio- and geophysical processes and change events, including natural and anthropogenic disturbances (Jin & Sader, 2005; Linderman et al., 2005; Zhang, Friedl & Schaaf, 2006). As part of this process, several vegetation indices (VI; Bayarjargal et al., 2006; Seiler et al., 2007; Verbesselt et al., 2009; Xiao et al., 2006) and products related to biophysical parameters such as leaf area index (LAI; Gao et al., 2008; Jiang et al., 2010) or primary productivity (Ricotta et al., 1999; Running et al., 2004; Verstraeten et al., 2010; Zhao et al., 2005) were used to study essential vegetation parameters over time. At the same moment, a variety of methods has been developed for classifying and detecting temporal changes in land surface properties (Coppin et al., 2004; Lu, Mausel, et al., 2003; Lu &

* Corresponding author. Tel.: +32 498569351.

E-mail address: stef.lhermitte@gmail.com (S. Lhermitte).

Weng, 2007; Mas, 1999; Singh, 1989). The application of these methods range from a point timescale (e.g., post-classification analysis of single date images and interpretation of the results over time) to a bi-temporal (e.g., bi-temporal change detection) and continuous timescale (e.g., classification and change detection based on temporal trajectory analysis).

Temporal trajectory analysis at a continuous timescale has been shown particularly useful to characterize land ecosystem dynamics, since it effectively exploits the multi-temporal sequence of images to reveal temporal patterns over several time scales (Bruzzone et al., 2003). On the intra-annual time scale, vegetative ecosystems typically show a seasonal temporal trajectory driven by plant phenologies affected by rainfall or temperature (Heumann et al., 2007; Zhang et al., 2003; Zhang et al., 2006) where different vegetation communities and plant species tend to respond differently (Hermance et al., 2007). Between years, these phenological cycles (e.g., onset and end of greenness, length of growing season) may alter which can be associated with seasonal changes (e.g., intra-annual changes related to plant phenology; Verbesselt et al., 2010a), gradual changes (e.g., inter-annual changes due to climate variability; Jacquin et al., 2010; Myneni et al., 1997; Tottrup & Rasmussen, 2004) and abrupt changes (e.g., natural or anthropogenic disturbances; de Beurs & Henebry, 2005; Verbesselt et al., 2009). Accordingly, the temporal trajectory has been utilized to characterize ecosystem dynamics and its changes have been used to identify, or discriminate among, land cover types and monitor land cover responses to inter-annual variability, climate, land use and disturbances (Bradley & Mustard, 2008; Hermance et al., 2007; Myneni et al., 1997; Zhou et al., 2001).

Time series similarity plays an important role in these methods for temporal trajectory analysis. First, time series similarity has been used as an absolute criterion to derive statistical inferences about the relationship between time series of different data sets (Bretherton et al., 1992; Tippett et al., 2008). In this context, a variety of methods have been applied in remote sensing studies to resolve the association between time series of remote sensing data, on one hand, and bio- and geophysical variables, on the other hand. These methods range from singular vector decomposition (SVD; Gong & Ho, 2003; Gong & Shi, 2004; Xiang & Liu, 2002) and canonical correlation analysis (CCA; Buermann et al., 2003; Castro et al., 2009; Lotsch et al., 2003) to more commonly employed methods based on regression and correlation analysis (Anyamba et al., 2001; Brown et al., 2006; Buermann et al., 2003; Gong & Ho, 2003; Gong & Shi, 2003; Gurgel & Ferreira, 2003; Herrmann et al., 2005; Huemmerich et al., 2005; Jiang et al., 2010; Los et al., 2001; Nezlin et al., 2005; Prasad et al., 2007; Sarkar & Kafatos, 2004; Studer et al., 2007; Verbesselt et al., 2006; Wang et al., 2005; White et al., 2009; Zhou et al., 2001).

Second, time series similarity has been employed as a relative criterion to numerically characterize the relationship between time series, not to derive statistical inferences, but to provide a decision criterion to cluster/discriminate time series. For example, in several classification approaches the similarity measures supply the premise to cluster the satellite pixel time series data in homogeneous groups based on minimization of within group temporal similarity and maximization of between group temporal similarity. The temporal behavior of these clusters can then serve to characterize and classify them (Azzali & Menenti, 2000; Brown et al., 2007; Defries et al., 1995; Friedl et al., 2010; Huang & Sieger, 2006; Lhermitte et al., 2008). In change detection approaches, on the other hand, the similarity measures allow to discriminate changes within one time series (e.g., the change in vegetation growth between different years; Bayarjargal et al., 2006; Lambin, 1996; Lambin & Strahler, 1994; Linderman et al., 2005; Vanacker et al., 2005).

Despite the generalized use of these time series similarity measures, there is no fixed definition of time series similarity (Liao, 2005). Accordingly, the remote sensing literature contains reference to a variety of strategies to evaluate time series similarity, ranging

from absolute similarity (e.g., SVD, CCA, regression and correlation analysis) to relative similarity measures such as distance measures (e.g., Euclidean distance; Lambin & Strahler, 1994), correlation measures (e.g., correlation coefficient; Geerken et al., 2005b), or principal component analysis (PCA; Eastman & Fulk, 1993), Fourier transform (Azzali & Menenti, 2000), and metric based measures (Lloyd, 1990). Many of these time series similarity measures do not differ from similarity measures used for other data series types (e.g., in the spectral or spatial domain) or from classical statistical analysis (e.g., regression analysis). Care should however be taken when applying these similarity measures as several of the underlying assumptions (e.g., stationarity, absence of serial correlation) are not always met or explicitly considered in real-world applications, resulting in an overestimated similarity (Bence, 1995; Granger & Newbold, 1974; Lin & Brannigan, 2003; Meek et al., 1999; Olden & Neff, 2001; Verbesselt et al., 2006; Yule, 1926). In this context, a variety of research and review papers have stressed the importance of understanding the evaluation criteria and temporal statistics in different domains ranging from pattern recognition (Halkidi et al., 2001; Liao, 2005) to climatology (Fovell & Fovell, 1993; Gong & Richman, 1995; Mimmack et al., 2001; Yiou et al., 1996; Zwiers & Von Storch, 2004) and oceanography (Mantua, 2004). Nevertheless, a quantitative study summarizing and comparing the existing similarity measures has not been performed. Gong and Richman (1995) and Mimmack et al. (2001) compared the frequently used Euclidean distance, Mahalanobis distance and correlation coefficient similarity and discussed the consequences of using PCA transforms, but did not incorporate the other similarity measures frequently used. However, with the growing importance of satellite time series data in support of research on climate change (Badeck et al., 2004; Potter & Brooks, 1998; White et al., 2005) and vegetation dynamics (Duchemin et al., 1999; Hill & Donald, 2003; Lu, Raupach, et al., 2003) there is a strong need for a more comprehensive understanding concerning the existent similarity measures. This understanding is specifically important since many of these similarity measures serve as underlying decision criterion in several time series clustering and change detection techniques and choice of the similarity may affect the final classification and change detection outcome (Mimmack et al., 2001).

This paper aims to address the current need for a more thorough comparison and a broader understanding of the available time series similarity measures used in classification and change detection approaches based on temporal trajectory analysis. The objectives were (i) to present an overview of the commonly used similarity measures that provide the decision criterion for these approaches, and (ii) to quantitatively compare the sensitivity of these measures in function of varying time series and ecosystem characteristics. To address these objectives, firstly the characteristics of multi-temporal remote sensing data and ecosystem dynamics are discussed and a summary of the commonly used similarity measures in remote sensing literature is presented (Section 2). Secondly, the performance of the commonly used similarity measures is quantitatively evaluated by means of Monte-Carlo simulations based on three data sets of global land ecosystems dynamics (Sections 3–5). Finally, the importance of ecosystem and time series characteristics for similarity measure selection is illustrated in a case study based on multi-temporal land cover classification (Section 6).

2. Background

The ability of any methodology to classify or detect changes in temporal trajectories depends on a variety of choices, where the selection of data (e.g., based on spatial, spectral, and temporal characteristics) and methodology (e.g., based on the characteristics of the time series similarity criterion) should be driven by the ecosystem dynamics one wants to discriminate in relation to the

variability one wants to identify or account for. In this context, this section gives an overview of some typical remote sensing data time series (Section 2.1), how they represent ecosystem characteristics (Section 2.2). Additionally, the theoretical background of previously applied time series similarity measure in remote sensing literature is given to provide a thorough comparison and broader understanding of their characteristics (Section 2.3).

2.1. Multi-temporal remote sensing data

2.1.1. Data characteristics

Several optical space-borne sensors with different temporal and spatial resolutions allow regular monitoring of the different temporal properties of ecosystem dynamics as they provide multi-temporal measurements of the land surface. In this context, sensors that provide data on an intra-annual time scale are particularly useful as they can be used to monitor the seasonal temporal trajectory driven by plant phenologies sometimes. These sensors may be separated based on their temporal and spatial characteristics for describing the ecosystem characteristics. First, several coarse to moderate spatial resolution sensors (0.25–1 km) with high temporal resolution (1–3 days), such as the Moderate Resolution Imaging Spectroradiometer (MODIS; Beck et al., 2006; Fensholt et al., 2004), Medium Resolution Imaging Spectrometer (MERIS; Dash et al., 2007; Dash et al., 2010), Advanced Very High Resolution Radiometer (AVHRR; Fensholt et al., 2006; Julien & Sobrino, 2009b; White et al., 2005), Advanced Along Track Scanning Radiometer (AATSR; Soria & Sobrino, 2007), and SPOT-Vegetation (VGT; Lhermitte et al., 2008; Verbesselt et al., 2007) have been proven useful for monitoring vegetation dynamics at regional to global scales. The main advantage of these sensors is the high temporal resolution of their observations, which allows to focus on the temporal trajectory. However, their rather coarse spatial resolution limits the spatial patterns that can be resolved, which makes them less suitable for use in small-structured ecosystems. In these cases, time series of higher spatial resolution data such Landsat TM/ETM+ (30 m) offer higher potential (Cohen & Goward, 2004), but their temporal coverage (16 days) in combination with possible cloud contamination (Ju & Roy, 2008) confines the image availability to a few scenes per year and this may limit the analysis of intra-annual dynamics (e.g., Lhermitte et al., 2011; Veraverbeke et al., 2010). Nevertheless, several authors successfully applied time series analysis techniques to Landsat data to assess intra-annual vegetation dynamics (Brown et al., 2006; Simonneaux et al., 2008; Vogelmann & DeFelice, 2003) instead of only focusing on inter-annual changes (Knudby et al., 2010; Lawrence & Ripple, 1999; Matricardi et al., 2010; Olthof et al., 2008; Röder, Hill, et al., 2008; Röder et al., 2008). Besides, the use of very high spatial data with high revisit capacities offers strong possibilities to monitor intra-annual dynamics. For example, FORMOSAT-2 provides images with daily observations and 2 m spatial resolution (Courault et al., 2008; Duchemin et al., 2008; Hadria et al., 2010), whereas IKONOS or Quickbird have below 1 m spatial resolution and can use their off-nadir viewing capacity to deliver images with a high temporal frequency.

Regarding spectral coverage, these sensors cover a variety of wavelengths useful to represent the ecosystem dynamics (Carrao et al., 2010; Kerr & Ostrovsky, 2003; Thenkabail et al., 2004). Moreover, a variety of biophysical parameters (e.g., LAI) and vegetation indices that relate to vegetation parameters (e.g., the commonly used Normalized Difference Vegetation index (NDVI) and Enhanced Vegetation Index (EVI)) have been derived from these spectral wavelength information to capture essential temporal vegetation properties such as green leaf biomass, LAI, percent green cover, and annual primary production (Bannari et al., 1995; Bayarjargal et al., 2006; Carlson & Ripley, 1997; Glenn et al., 2008; Huete et al., 1997; Huete et al., 2002; Justice & Hiernaux, 1986; Kerr & Ostrovsky, 2003; Pettoirelli et al., 2005; Seiler et al., 2007).

2.1.2. Time series characteristics

The spatial, spectral, and temporal characteristics of the remote sensing data results in time series data, whose characteristics (e.g., serial correlation, stationarity, temporal resolution, noise, unequally spaced observations or missing values) will affect the performance of any classification or change detection approach (Mimmack et al., 2001).

- Serial correlation occurs when time series values are correlated between different temporal observations within one time series. This type of correlation in ecosystem time series is mainly caused by the seasonal variation of vegetation (Zoffoli et al., 2008), where temporal observations are not independent and may contribute overlapping information gain (Carrao et al., 2008).
- Time series stationarity, i.e. invariance of statistical properties over time (Davis et al., 1994; Lin & Brannigan, 2003), is another important characteristic that may affect the similarity measure performance. For example, temporal observations with larger variance may dominate the behavior of several similarity measures when the time series' variance is not constant over time (Jain et al., 1999).
- Temporal resolution is another important factor as the time interval between consecutive observations can vary significantly. This can be due the sensor characteristics (e.g., daily MODIS vs. 16-day Landsat images), but can also be the result of pre-processing steps such as compositing. Compositing is a process that selects for each pixel the best observation among all available within a period of time based on cloud-free properties or an alternative maximization of desired signal (Cihlar et al., 1994; Holben, 1986; Viovy et al., 1992). Temporal resolution will determine the serial correlation between temporal observations and the temporal detail that can be distinguished. For rapidly changing dynamics, a high temporal resolution will be essential (Lhermitte et al., 2011; Veraverbeke et al., 2010), whereas for observations with high serial correlation using more observations will contribute less to the overall performance (Carrao et al., 2008).
- Noise in the satellite time series may be the result of varying atmospheric conditions, sun-sensor-surface viewing geometry, sensor disturbances, geometric errors, misregistration, mixed pixels, surface anisotropy, and clouds or cloud shadows (Hird & McDermid, 2009; Jönsson & Eklundh, 2004). Although all these noise components reduce the signal to noise ratio (SNR), their effect may be very different. For example, the simultaneous presence of several uncorrected noise components (e.g., geometric errors, sub-resolution changes, or atmospheric conditions; Fig. 1b) may cause false highs and lows which are often assumed to be random or white noise (Lucht & Lewis, 2000; Vasseur & Yodzis, 2004). Cloud cover, snow or shadow, on the other hand, shows a typical effect of increased or decreased observation values (e.g., increase in blue reflectance and decrease in NDVI) and therefore introduces positively or negatively biased errors (e.g., Fig. 1c). This results in a biased error structure, where, for example, high values are more trustworthy than low ones in NDVI time series (Chen et al., 2004; Jönsson & Eklundh, 2002; Roerink et al., 2000). Moreover, other noise models might affect the time series data (e.g., long term trend due to sensor drift). Consequently, an understanding of noise properties is essential (e.g., noise color; Vasseur & Yodzis, 2004).
- Unequally spaced observations or missing values often occur in satellite time series. For example, not all satellites have regular revisit times or cloud cover can result in a number of consecutive missing values in the time series of satellite data, causing unequally spaced observations of valid data (Ju et al., 2010).

Due to the impact of these characteristics on any many classification or change detection approach, adequate pre-processing steps are often essential. Among others these steps may include: (i) the extraction of non-serially correlated metrics to avoid serial correlation

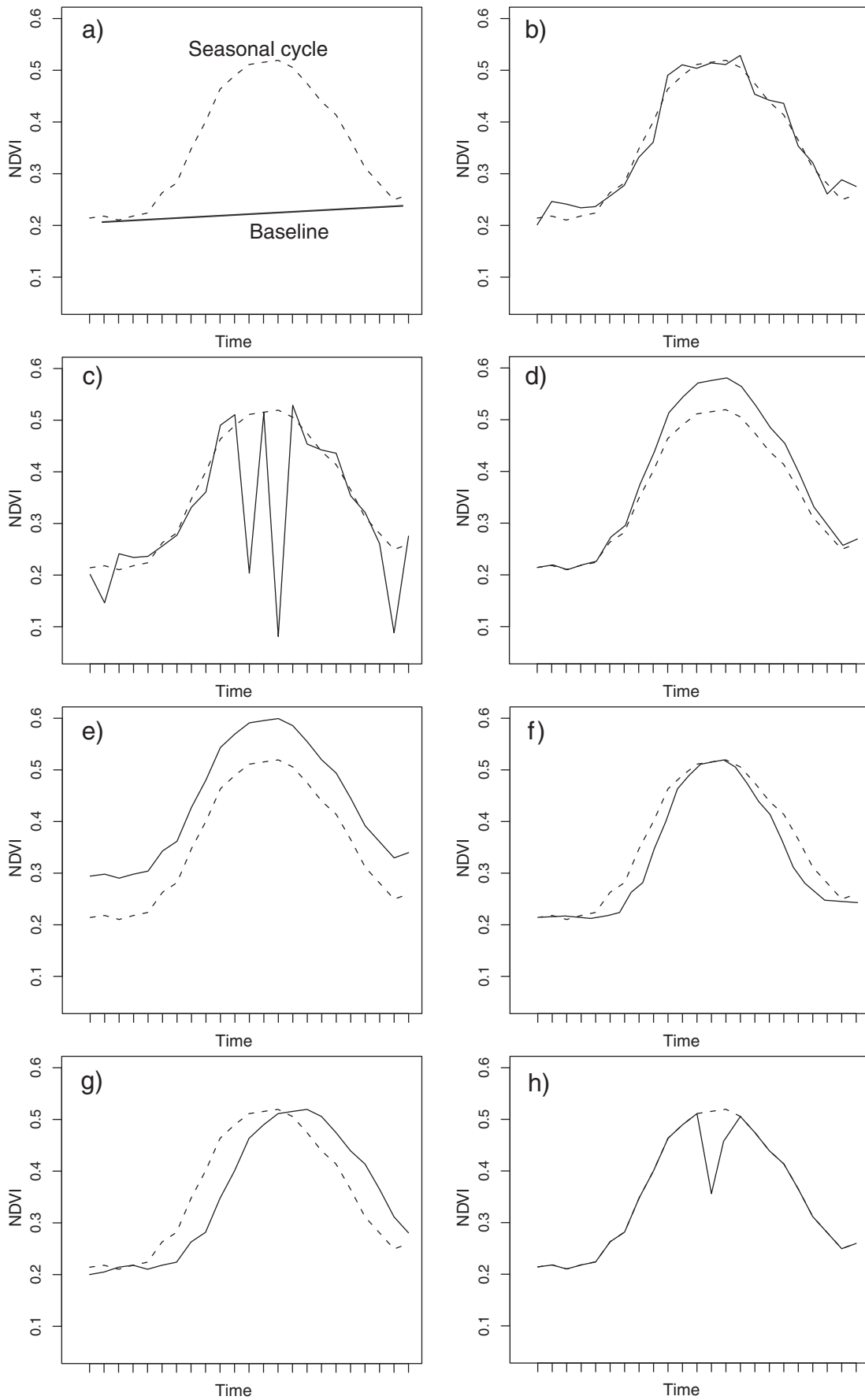


Fig. 1. Illustration of time series characteristics and ecosystem dynamics: a) temporal trajectory characterized by baseline and seasonal phenological cycle; b) white or random noise; c) biased noise; d) amplitude scaling; e) amplitude translation; f) time scaling; g) time translation; and h) shape changes.

(Sakamoto et al., 2005; Verbesselt et al., 2006; Verbesselt et al., 2006), (ii) the differencing of observations to remove non-stationarity (Verbesselt et al., 2009), (iii) the application of atmospheric correction, normalization or bidirectional reflectance distribution function (BRDF) corrections to minimize noise effects (Ju et al., 2010; Latifovic et al., 2003; Vermote et al., 2009), (iv) compositing to minimize cloud effects and obtain equally spaced observations that are less affected by serial correlation (Cihlar et al., 1994; Holben, 1986; Viovy et al., 1992), and (v) the application of interpolation or curve fitting techniques to remove spurious observations, interpolate missing values, and obtain equally spaced observations (Chen et al., 2004; Jönsson & Eklundh, 2004; Julien & Sobrino, 2009a; Kang et al., 2005; Roerink et al., 2000).

2.2. Ecosystem characteristics

An understanding of how ecosystem dynamics affect the seasonal temporal trajectory is crucial before specifying the ecosystem variability one wants to identify. Generally, these temporal trajectories are characterized by a baseline (e.g., due to soil background or understory vegetation out of the growing season) and a seasonal phenological cycle (Fig. 1a) with a vegetation specific amplitude (defined as the difference between the seasonal peak of the time series and the baseline), timing (defined as the time location of the seasonal peak of the time series due to timing of green-up and senescence), and shape (e.g., due to rate of green-up and senescence and intra-seasonal variability). Changes in ecosystem dynamics can consequently affect the baseline, amplitude, timing, and shape characteristics of the time series, resulting in amplitude effects (i.e., amplitude scaling and translation), timing effects (i.e., time scaling and translation), or shape effects.

Amplitude effects result in changes in the difference between the seasonal peak of the time series and the baseline. Amplitude scaling can be compared to intensity variations and occurs when the seasonal peak has been stretched or compressed in the y-axis (Fig. 1d). Myneni et al. (1997), Eklundh and Olsson (2003), Geerken et al. (2005b), and Heumann et al. (2007) illustrated for NDVI time series that amplitude scaling could be related to changes in vegetation vigor or coverage, changing the height peak of the NDVI curve. Amplitude translation (i.e., when the time series has been shifted in the y-axis; Fig. 1e), on the other hand, was related to shifts in the baseline or background reflectance (Geerken et al., 2005b). Eklundh and Olsson (2003) and Heumann et al. (2007), moreover, related reduced amplitudes to a combined effect of amplitude scaling and translation in wetter regions, as they noticed an increase in minimum seasonal NDVI and no change in maximum seasonal NDVI due to saturation at high vegetation densities. This results in a NDVI temporal trajectory with higher baseline (i.e., positive amplitude translation) and lower amplitude range (amplitude scaling factor < 1).

Timing effects occur when the time location of the seasonal peak of the time series has changed. For example, time scaling (i.e., when the time series has been stretched or compressed in time, changing the width of the seasonal trajectory; Fig. 1f) has been associated by Reed et al. (1994), Eklundh and Olsson (2003), Hill and Donald (2003), Heumann et al. (2007), and Wardlow et al. (2007) to changes in the length of the growing season. Additionally, they demonstrated that time translation (i.e., when the time series has been shifted in time without changing the width of seasonal trajectory; Fig. 1g) would occur primarily due to a change of the raining season, resulting in an earlier or later onset of the growing season but similar length of the growing season.

Shape effects arise when the shape of temporal profile has been changed. These can be the result of amplitude or timing effects (e.g., time scaling clearly affects the shape of the temporal profile), but can also be the result of other types of change (e.g., disturbances, land cover/land use change) that have no determined scaling or translation

effect on the time series. For example, Evans and Geerken (2006) used a classification algorithm for vegetation types or land use practices that is invariant to variations in amplitude scaling, amplitude translation and time translation, that may be caused by differences in climate, background or topography, but are unrelated to the vegetation type. Verbesselt et al. (2010a), Verbesselt et al. (2010b), Lhermitte et al. (2011), and Veraverbeke et al. (2010), on the other hand, used shape changes of the temporal trajectory to study changes in the vegetation type and its properties.

2.3. Time series similarity measures

Finally, the knowledge of data characteristics and ecosystem dynamics one wants to discriminate will determine the selection of the time series similarity measure, represented by D , that provides the decision criterion for the classification or change detection approach. These D can be grouped into three major categories depending upon whether they work (i) directly with original time series data, (ii) indirectly with transformations extracted from the original time series data, or (iii) indirectly with metrics derived from the original time series data. An additional overview of the D 's discussed here is given in Table 1.

2.3.1. Original time series data approaches

The original time series data approaches calculate D directly from the original time series value without applying any transformation to the data. Here, two approaches can be distinguished: (i) distance and (ii) correlation measures.

2.3.1.1. Distance measures. The most commonly used distance measures in classification or change detection approaches are derived from the Minkowski distance (D_{Mink} ; Jain et al., 1999), as it is a generalization of both the Euclidean distance (D_E) and the Manhattan distance (D_{Man}). The Minkowski distance between two individual time series $f^p(t)$ and $f^q(t)$ collected in time t , for pixels p and q respectively, is given by:

$$D_{Mink} = \left(\sum_{t=1}^N |f_t^p - f_t^q|^r \right)^{\frac{1}{r}} \quad (1)$$

where f_t^p is the $f^p(t)$ time series value at moment t and N is the number of samples in the time series and r is a user defined integer. With $r = 1$, Eq. (1) defines the Manhattan distance D_{Man} , whereas $r = 2$ produces the Euclidean distance D_E , which is more sensitive to outlier values (e.g., noise) due to its non-linear character. The main advantage of the Minkowski distances is that they are easy to calculate and interpret. Therefore, they have been applied in a variety of approaches, ranging from change vector analysis (Bayarjargal et al., 2006; Friedl et al., 2002; Lambin & Ehrlich, 1997; Lambin & Strahler, 1994; Linderman et al., 2005; Serneels et al., 2007) to landcover classification (Brown et al., 2007; Huang & Sieger, 2006; Loveland et al., 2000; Simoniello et al., 2008; Viovy, 2000; Xia et al., 2008), where D_E often provides the similarity measure that is evaluated in several clustering algorithms (ISODATA, K-means, minimum distance). The Minkowski distances do not take into account the time interval between measurements, allowing them to be applied to unequally spaced observations (e.g., in a Landsat time series). Moreover, standardized Minkowski distances have been calculated that take into account the amount of observations (Liao, 2005). This allow to compare time series of unequal length and with missing values. Soudani et al. (2008), Lhermitte et al. (2010), Lhermitte et al. (2011), and Veraverbeke et al. (2010), for example, calculated D_E based on only corresponding observations (N') in time series with missing data and subsequently divided D_E by N' .

Table 1
Summary of time series similarity measures D .

D	Characteristics	Examples
D_{Man}	Quantifies the absolute magnitude of the difference between time series	Modified version of temporal change vector (Bayarjargal et al., 2006; Linderman et al., 2005; Serneels et al., 2007)
D_E	Quantifies the Euclidean distance of the difference between time series	Classical temporal change vector (Bayarjargal et al., 2006; Friedl et al., 2002; Lambin & Ehrlich, 1997; Lambin & Strahler, 1994), minimum distance classification (Brown et al., 2007; Loveland et al., 2000), ISODATA classification (Huang & Sieger, 2006; Xia et al., 2008), K-means classification (Simoniello et al., 2008) and classification (Viovy, 2000), control pixel selection (Lhermitte et al., 2010; Veraverbeke et al., 2010)
D_{Mah}	Quantifies the difference between time series but accounts for non-stationarity of variance and temporal cross-correlation	Maximum likelihood classification (Bergen et al., 2005; Defries & Townshend, 1994; Ehrlich & Lambin, 1996; Veraverbeke et al., 2010), Mahalanobis change vector (Bontemps et al., 2008)
D_{CC}	Quantifies the degree of linear relationship between time series	Correlation based classification (Brown et al., 2007; Geerken et al., 2005a,b), control pixel selection (Lhermitte et al., 2010), cross-correlogram spectral matching (Van der Meer & Bakker, 1997; Wang et al., 2009)
D_{PCA}	Quantifies the difference between times PCs that explain the majority of the variance	Benedetti et al. (1994) and Lobo and Maisongrande (2008)
D_{FFT}	Quantifies the combined effect of FT amplitude and phase differences	ISODATA and minimum distance classification based on FT components (Azzali & Menenti, 2000; Moody & Johnson, 2001; Wagenseil & Samimi, 2006)
D_ξ	Quantifies shape similarity based on derived FT amplitude and phase differences	Classification (Evans & Geerken, 2006)
D_{FK}	Quantifies the FT of the difference between time series	Hierarchical image segmentation (Lhermitte et al., 2008)
D_Δ	Quantifies the difference between time series based on specific designed metrics	Metric change detection (Borak et al., 2000; Linderman et al., 2005), classification and regression trees (Hansen et al., 2003; Lloyd, 1990)

Although the Minkowski distances are mathematically simple, they have certain limitations. Most importantly, they do not account for non-stationarity of variance or temporal cross-correlations in the data set (Mimmack et al., 2001). As a result, the observations with the largest variance (if not standardized) will dominate Eq. (1) as they contribute more strongly to the similarity (Jain et al., 1999). Solutions to this include the use of the Mahalanobis distance (D_{Mah} ; Mahalanobis, 1936):

$$D_{Mah} = \sqrt{(f_t^p - f_t^q)^T \Sigma^{-1} (f_t^p - f_t^q)} \quad (2)$$

where Σ is the covariance matrix of the time series, which needs to be estimated beforehand. The assumption behind the D_{Mah} is that all points in the data set have temporal distributions that can be represented by Σ . Since this is not generally true, most studies calculated Σ of each class or category separately and used D_{Mah} as the probability of belonging to a class. Using this probabilistic interpretation, it corresponds to selecting the class with maximum likelihood and D_{Mah} provides the similarity measure for the maximum likelihood classifier. Defries and Townshend (1994), Ehrlich and Lambin (1996),

Bergen et al. (2005), and Veraverbeke et al. (2010) used this approach to classify land cover using VI time series, whereas Carrao et al. (2008) used D_{Mah} to determine optimal band-timing combinations for land cover classification. Bontemps et al. (2008), on the other hand, used D_{Mah} to calculate the distance from an unchanged reference to quantify the probability of change. The drawback of D_{Mah} is the need of prior information on the covariance matrix. This means that one needs to estimate the covariance matrix of the data or of each class/category beforehand. This estimation is usually based on samples known to belong to each class or category (e.g. after a supervised classification).

2.3.1.2. Correlation measures. The best known correlation measure is Pearson's cross-correlation (D_{CC}) coefficient (Liao, 2005; Rodgers & Nicewander, 1988), which is defined as the degree of linear relationship between time series:

$$D_{CC} = \frac{\sum_{t=0}^{N-1} [(f_t^p - \bar{f}^p) * (f_{t-s}^q - \bar{f}^q)]}{\sqrt{\sum_{t=0}^{N-1} (f_t^p - \bar{f}^p)^2} * \sqrt{\sum_{t=0}^{N-1} (f_{t-s}^q - \bar{f}^q)^2}} \quad (3)$$

Where f_t^p and f_t^q are the time series values at moment t , f^p and f^q are the means of the corresponding series, s is the lag between both time series, and N is the length of the time series. If D_{CC} is computed for $s=0$, it estimates the time series similarity without time shift. When D_{CC} is calculated for one time series, i.e. when $f^p(t) = f^q(t)$, it measures the serial correlation (Meek et al., 1999). D_{CC} is 1 in case of an increasing linear relationship, -1 in case of a decreasing linear relationship, and some value in between in all other cases. Since D_{CC} is a measure of a linear relationship between time series and does not evaluate the difference in time series values, amplitude scaling or translation will not affect D_{CC} .

D_{CC} is often used as an similarity measure for remote sensing time series. Geerken et al. (2005a) and Geerken et al. (2005b), for example, used D_{CC} between NDVI time series as a measure to classify the spatial coverage variations of rangeland vegetation, whereas Lhermitte et al. (2010) applied it for control pixel selection and Brown et al. (2007) added it as a measure to classify crop types. Van der Meer and Bakker (1997) based the cross correlogram spectral matching (CCSM) classification on correlation between spectra at different s and Wang et al. (2009) applied it to NDVI time series data for identifying interannual landcover changes.

2.3.2. Transformation approaches

The transformation approaches apply a transformation (e.g., principal component analysis (PCA) or Fourier transform (FT)) on the time series to assess similarity. Generally, this transformation has two objectives: (i) to reduce the dimension of the time series without losing too much information, and (ii) to isolate some specific components.

2.3.2.1. PCA. PCA was first introduced by Pearson (1901), and developed independently by Hotelling (1933). Its background and applications is extensively discussed in Jackson (1991) and Jolliffe (2002). PCA transforms the time series data of the original multi-temporal space to a new uncorrelated coordinate space, so that the largest variance is located on the first coordinate (called the first principal component), the second largest variance on the second coordinate, and so on. This can be done by using standardized and unstandardized principal component analysis, where the former allows to solve non-stationarity of variance. Because of the maximization of the variance in the first components, PCA allows data reduction when retaining only those characteristics of the data set that contribute most to its variance. Moreover, for some applications it

allows to relate specific principal components (PC) to specific phenomena based on empirical analysis.

PCA has been widely used in remote sensing studies to isolate specific components related to vegetation dynamics (Anyamba & Eastman, 1996; Eastman & Fulk, 1993; Gurgel & Ferreira, 2003; Hall-Beyer, 2003; Hirosawa et al., 1996) or to perform classification based on time series similarity (Benedetti et al., 1994; Lobo & Maisongrande, 2008). In the latter context, PCA is used as a way of dimensionality reduction before calculating the similarity between m selected PCs:

$$D_{PCA} = \sqrt{\sum_{k=1}^m (PC_k^p - PC_k^q)^2} \quad (4)$$

where PC_k^p and PC_k^q are the k th principal component of time series p and q , respectively, and m is the number of selected principal components.

One of the main advantages of the D_{PCA} is the transformation to successive components that explain progressively less of the total data set variance. Usually, high order components will contain information that is essentially noise with respect to the phenomenon analyzed (Jackson, 1991; Jolliffe, 2002), and so can be disregarded when calculating D_{PCA} . Additionally, noise elements such as long-duration cloud events or sensor and processing problems are likely to be isolated in their own components, and thus may be more easily separated from the desired signal (Hall-Beyer, 2003). However, it is always possible that some high order component, containing a very low proportion of total data set variance, might represent informational variance for a small area. Therefore the selection of m PCs is an essential step as it will determine the output of all algorithms that use the D_{PCA} (Mimmack et al., 2001). Several of these selection approaches are discussed in Jackson (1991) and Jolliffe (2002).

2.3.2.2. Fourier transforms. Also the FT has been frequently used for similarity assessment of ecosystem dynamics, since it allows the decomposition of noise-affected time series into periodic signals in the frequency domain. By performing the analysis in the frequency domain, a distinction can be made between signals with a specific period such as frequency terms related to vegetation dynamics and other frequency terms (Azzali & Menenti, 2000; Canisius et al., 2007; Jakubauskas et al., 2002).

The FT can be used to transform any equidistant discrete time series $f(t)$ into a set of scaled cosine waves with unique amplitude A_k and phase shift ϕ_k (Bracewell, 2000):

$$f(t) = A_0 + \sum_{k=1}^{N-1} A_k \cos(2\pi kt + \phi_k) \quad (5)$$

with

$$A_k = \sqrt{F_k^c{}^2 + F_k^s{}^2} \quad (6)$$

and

$$\phi_k = \arctan\left(\frac{F_k^c}{F_k^s}\right) \quad (7)$$

where t is an index representing the sample moment, f_t is the time series value at moment t , k is the frequency of the FT components (i.e., the number of cosine wave cycles over the time series), N is the number of samples in the time series, F_k^c and F_k^s are the real and imaginary part in Euler's equation, respectively. Together A_k and ϕ_k describe the k th frequency FT component as one cosine wave in the frequency domain, whereas the sum of the cosine waves represents the original time series of each pixel (Bracewell, 2000).

Several authors have used the FT of VI time series as the basis for time series similarity assessment. Firstly, Azzali and Menenti (2000)

suggested a distance measure based on the Euclidean distance between m selected amplitude and phase components of the fast Fourier transform (D_{FFT}):

$$D_{FFT} = \sqrt{\sum_{k=0}^m (A_k^p - A_k^q)^2 + \sum_{k=1}^m (\phi_k^p - \phi_k^q)^2} \quad (8)$$

Since D_{FFT} incorporates amplitude and phase, it is sensitive to amplitude scaling, time scaling and time translation. The sensitivity to amplitude translation will depend on the inclusion of the 0th FT component in the D_{FFT} , since this component represents the mean of the time series. Azzali and Menenti (2000) used the amplitude and phase of the 0th, 1st, and 2nd FT components of one year NDVI time series to classify vegetation–soil–climate units. Moody and Johnson (2001) and Wagenseil and Samimi (2006) also used the 0th, 1st, and 2nd FT components, but they focused on two and five year NDVI time series.

Secondly, Evans and Geerken (2006) proposed a distance measure D_ξ that mainly quantifies shape similarity:

$$D_\xi = 3\sqrt{\sum_{k=1}^m (\alpha_k^{ref} - \alpha_k)^2 + \sum_{k=1}^m (\theta_k^{ref} - \theta_k)^2} \quad (9)$$

where α_k and θ_k are the relative amplitude and phase for each FT component:

$$\alpha_k = \frac{A_k}{A_1} \quad (10)$$

and

$$\theta_k = \left(\frac{A_k}{A_1}\right)_{ref} [2 + \cos(k\phi_1 - \phi_k)] \quad (11)$$

and α_k^{ref} and θ_k^{ref} are relative amplitude and phase for a reference class. D_ξ is zero if two time series, represented by their m Fourier components, have the same shape and increases as the differences between the shapes increases. Due to the use of the relative amplitude and phase, D_ξ is invariant to amplitude translation, amplitude scaling and time translation. This invariance was necessary for Evans and Geerken (2006) as they focused on shape similarity for classifying rangeland without taking modifications related to a plant phenology into account.

Finally, Lhermitte et al. (2008) proposed a F_k -distance criterion (D_{Fk}) for hierarchical image segmentation based on time series similarity. This criterion employs the Euclidian distance between FT components of the same frequency as measure of similarity. The dashed line A_k^{p-q} in Fig. 2 illustrates D_{Fk} for the k^{th} frequency FT component of two time series, represented by p and q . The F_k -distance incorporates both parameters that represent the FT component, A_k and ϕ_k , respectively, into one similarity measure. Mathematically, D_{Fk} corresponds to subtracting two time series, $f^p(t)$ and $f^q(t)$, respectively, for each observation in the temporal sequence and using the amplitude of the resulting difference vector $f^{p-q}(t)$:

$$A_k^{p-q} = \sqrt{(F_k^c(p) - F_k^c(q))^2 + (F_k^s(p) - F_k^s(q))^2} \\ = \sqrt{F_k^c(p-q)^2 + F_k^s(p-q)^2} \quad (12)$$

Based on the A_k^{p-q} of the selected m FT components, D_{Fk} can be calculated:

$$D_{Fk} = \sum_{k=0}^{N-1} w_k A_k^{p-q} \quad (13)$$

where A_k^{p-q} is the F_k -distance between the time series of p and q respectively, and w_k is the weight of the k^{th} frequency FT component.

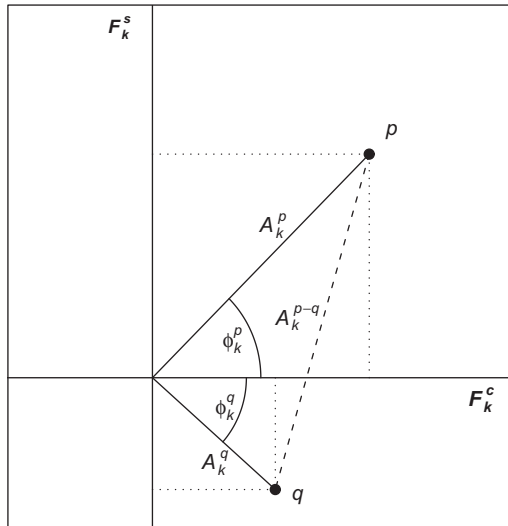


Fig. 2. Illustration of the F_k -distance for the k th frequency FT components of two time series, represented by p and q . F_k^c and F_k^s are amplitudes of the cosine and sine waves in rectangular notation, while A_k and ϕ_k are the amplitude and phase in polar notation, respectively. A_k^{p-q} is the distance between points p and q used in the F_k -distance criterion.

Modification of the weights allows to enhance (high w_k) or diminish (low w_k) the influence of each component on D_{Fk} and to accentuate specific components in the similarity measure. As a result, these weights will determine the sensitivity to time series differences. For example, when $w_0=0$ the D_{Fk} will be insensitive to amplitude translations as the offset value in the y -axis is neglected in the D_{Fk} calculation.

The main advantage of all these FT distances is the possibility to distinguish signals with a specific period. This is particularly amendable for detecting periodic patterns in time series of satellite data, such as daily or monthly time series of land surfaces that contain strong systematic periodic patterns related to vegetation features and nonsystematic high frequent image noise. Hence, information related to temporal vegetation characteristics can be separated from noise originating from atmospheric and viewing angle effects, cloud contamination, and other types of high frequency factors. This noise separation is also one of the main arguments in [Moody and Johnson \(2001\)](#), [Evans and Geerken \(2006\)](#), [Wagenseil and Samimi \(2006\)](#), and [Lhermitte et al. \(2008\)](#) for their choice for the FT approach. However, care should be taken as the assumption of a periodic and sinusoidal signal is often not satisfied for the complex shape of ecosystem dynamics, and FT analysis may therefore require high frequency terms for suitable approximation ([Wagenseil & Samimi, 2006](#)). Moreover, the separation between signal and noise will always depend on the appropriate selection of the m components or weights w_k .

2.3.3. Metric approaches

The metric approaches convert the raw data time series into a number of parameters that describe the time series in function of simple statistics, and subsequently calculate similarity based on these statistics. For ecosystem time series these metrics typically represent some aspects of timing, duration and intensity of photosynthetic activity (e.g., begin of the growing season, end of the growing season, annual mean, maximum, minimum, range, etc.; [Borak et al., 2000](#); [Defries et al., 1995](#); [Hill & Donald, 2003](#); [Lloyd, 1990](#); [Pettorelli et al., 2005](#); [Reed et al., 1994](#); [Samson, 1993](#); [White et al., 2009](#); [Zhang et al., 2003](#); [Zhang et al., 2006](#)). Although these metrics are excellent descriptions of a particular time series phenomenon, they provide characteristics that are not inter-comparable as they represent

different characteristics on different scales. Consequently, adapted scale invariant similarity measures must be used.

[Defries et al. \(1995\)](#) and [Hill and Donald \(2003\)](#) proposed an unsupervised classification procedure based on the Mahalanobis distance between several metrics in a maximum likelihood classifier. Alternatively, [Borak et al. \(2000\)](#) proposed the use of the distance between individual metrics (e.g., $D_\Delta = \text{metric}(f_t^p) - \text{metric}(f_t^q)$). This approach is very useful for detecting specific differences between time series. [Linderman et al. \(2005\)](#), for example, used the D_Δ of integrated EVIs to distinguish phenology differences from other changes. [Borak et al. \(2000\)](#) showed moreover that the combination of several D_Δ s of individual metrics performed better to discriminate between changes. [Lloyd \(1990\)](#) and [Hansen et al. \(2003\)](#) combined also several D_Δ s in their classification and regression trees.

One of the main advantages of the metrics based similarity is that they can be designed completely according to user requirements. For example, if one is interested in the length of the growing seasons, it is possible to design a metric that calculates begin and end of the growing season and to use the D_Δ of these metrics as indicator of time series similarity. On the other hand, this user input is also the main disadvantage, since external knowledge is essential to interpret the results.

3. Methods

To address the objective of quantitative comparison of the different D s, a sensitivity analysis based on Monte Carlo (MC) simulations was performed using three data sets (NDVI, EVI, and LAI) of global land ecosystem dynamics. The MC simulations allow to control the variability in time series and ecosystem characteristics, which is difficult when analyzing actual ecosystem time series where the variability of these characteristics is generally predetermined. As a result, the MC simulations provide a means to assess the sensitivity of each D in function of varying degrees of amplitude, timing and noise effects.

3.1. Satellite time series data

The global land ecosystem time series data were derived from the MODIS Land Product Subsets based on the MODIS ASCII Subset for the northern hemisphere ([Oak Ridge National Laboratory Distributed Active Archive Center \(ORNL DAAC\), 2010](#)), where the 2001–2006 Terra MODIS Landcover (MCD12Q1), NDVI (MOD13Q1), EVI (MOD13Q1) and LAI (MOD15A2) products for 7×7 km areas around 1085 flux towers or field sites in the northern hemisphere were selected ([Fig. 3](#)). The MCD12Q1 data provide annual estimates of the 17-class International Geosphere–Biosphere Programme classification (IGBP) landcover (LC) type ([Friedl et al., 2002](#); [Friedl et al., 2010](#); [Loveland et al., 1995](#)) for 14×14 0.5 km pixels around each flux tower or field site, whereas the MOD15A2 represents LAI estimates for the same sites based on 7×7 1 km pixels with 8-day temporal resolution, and the MOD13Q1 produces the site's NDVI and EVI values with a 16-day temporal resolution for 28×28 0.25 km pixels.

Based on the MCD12Q1 data, a dominant LC type was determined for each of the 1085 sites. Subsequently, the NDVI, EVI, and LAI time series were extracted that correspond to the dominant LC type for each site, resulting in a set of n_{LC} sample time series per IGBP landcover type. The five year NDVI, EVI and LAI data (2001–2006) were subsequently divided in annual time series and all subsequent analysis was based on annual time series and repeated for each year in 2001–2006. This annual approach allows to assess the dependence of the results on the annual variability.

The time series of NDVI, EVI and LAI data were assumed to typify each LC type, and, therefore, to represent global land ecosystem vegetative cover dynamics. Since NDVI, EVI, and LAI data show a different sensitivity to ecosystem vegetative cover dynamics, the use

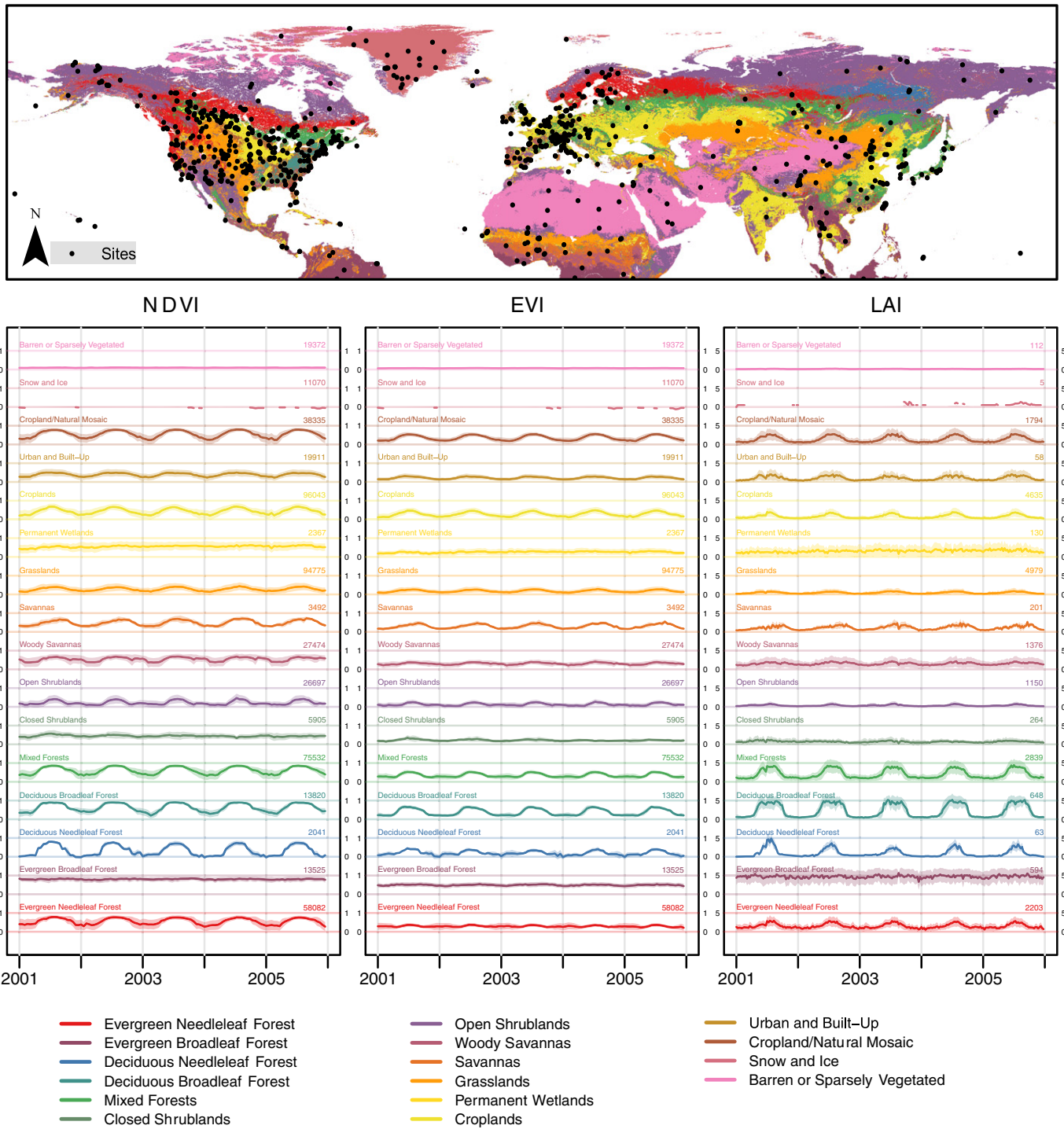


Fig. 3. Illustration of the MODIS ASCII Subset data for the northern hemisphere, representing the 2001–2006 Terra NDVI, EVI, and LAI products for 7×7 km around 1085 flux towers of field sites. The • illustrates the location of the 1085 flux towers of field sites in the different LC types, represented by different colors. The time series of NDVI, EVI, and LAI show the mean \pm standard deviation for each LC type, whereas the upper-right corner of each time series indicates n_{LC} , the number of sample time series per LC type in the data set.

of these three data sets allows moreover to compare the effect of different time series characteristics (temporal resolution, serial correlation, variance) on the sensitivity of D . This difference in sensitivity is apparent in Fig. 3 where the mean of the NDVI, EVI, and LAI time series for each LC type is represented. The NDVI has a higher range than EVI, but EVI tends to saturate at higher LAIs allowing more accurate change detection in high density vegetation (Huete et al., 2002). The LAI time series, on the other hand, show the highest variability (between 0 and 5) and also shows the most abrupt changes at the beginning and end of the growing season. Comparison of the

mean NDVI, EVI, and LAI times shows moreover that the amplitude, baseline, timing of on-set and end of the seasonal cycles clearly varies for LC types.

3.2. Time series properties

Since the performance of each D depends on the characteristics of the time series data, descriptive statistics of the time series were derived to understand the sources of variation in the sample time series of each LC type. This includes analysis of the mean and variance

per LC type over time, since these exemplify the variation related to baseline, amplitude, timing, and give insight in the phenological variability. Moreover, the serial correlation is derived to understand the effect of timing effects on the MC simulations.

3.3. Time series similarity measures

Eight relative time series similarity measures (D_{Mam} , D_E , D_{Mah} , D_{CC} , D_{PCA} , D_{FFT} , D_ξ , D_{Fk}) were compared in the sensitivity analysis. These D span the key concepts behind time series similarity and consequently allow to determine the different aspects of sensitivity. The metric based similarity measures were not included in this comparison, since they depend entirely on the users requirements and related definition of the metric (e.g., Defries et al., 1995). Therefore, comparing these metrics would result in comparing user definitions based on subjective selection criteria, which is beyond the scope of this study.

D_{Mam} , D_E , and D_{CC} were calculated using the individual annual time series, whereas the D_{Mah} was computed after estimating the covariance matrix of each LC type. D_{PCA} , D_{FFT} , D_ξ and D_{Fk} were computed based on the components that explain the majority of the intra-annual ecosystem variability. For D_{PCA} this implies the use of the three first standardized PCs, whereas the D_{FFT} , D_ξ and D_{Fk} were calculated based on the mean component ($k=0$) and on the components with annual and bi-annual frequency ($k=1, 2$). The D_{Fk} applied equal weights to each Fourier component ($w_k=0.33$; $k=0, 1, 2$).

3.4. Monte Carlo simulation experiment

As a basis for the MC simulations, characteristic NDVI, EVI, and LAI time series for each LC type (except for the Snow and Ice class, where too few observations were available) were derived based on the n_{LC} sample NDVI, EVI and LAI time series per LC type. This was done by (i) taking all observations with good quality (based on the associated data quality control flag) for each date and LC type, (ii) calculating the mean and standard deviation for the NDVI, EVI, and LAI time series for each date and LC type, and (iii) interpolating the mean and standard deviation for specific observation dates where no data were available. Based on the time series of the mean $\bar{f}^{LC}(t)$ and standard deviation $\sigma^{LC}(t)$ for NDVI, EVI and LAI data for each LC type, sample time series of each LC type can be generated using the equation proposed by Viovy (2000):

$$f^{LC}(t) = \bar{f}^{LC}(t) + \alpha \sigma^{LC}(t) \tag{14}$$

where α is a random value given by a pseudo-random generator that follows a standard normal distribution $N(\mu=0, \sigma=1)$. The use of $\bar{f}^{LC}(t)$ removes noise in the time series data due to its mean filter effect, whereas the use of α allows to represent the variability around the mean time series.

Subsequently, MC simulations were undertaken to introduce amplitude scaling and translation, time scaling and translation, and

noise in the characteristic NDVI, EVI, and LAI time series of each LC type. This was done by taking a simulated time series of Eq. (14) and modifying it using the simulation equations of Table 2. Amplitude scaling was consequently introduced by multiplying the time series of Eq. (14) with β , where w_{Asc} will determine how strong the scaling effect is. Amplitude translation, on the other hand, was added by introducing a random offset value, where w_{Ash} determines the offset. Time scaling was introduced elongating/shortening the original time series with β observations, where $-w_{Tsc} < \beta < w_{Tsc}$. This results in sample data sets where, for $w_{Tsc} = 1$, time series are scaled randomly one observation value, whereas for higher values of w_{Tsc} this scaling differs randomly between $-w_{Tsc}$ and w_{Tsc} observation values. For the elongated time series interpolation was used for observations in the middle of the time series. For the shortened time series, on the other hand, extrapolation based on previous year or next year observation values was used. Time translation was introduced by applying random shifts time to the sample time series of Eq. (14), where $-w_{Tsh} < \beta < w_{Tsh}$ determines the shift. As a result, time series are shifted randomly one observation value for $w_{Tsh} = 1$, whereas for higher values of w_{Tsh} this shift differs randomly between $-w_{Tsh}$ and w_{Tsh} observation values. For each of these shifts, the same extrapolation technique as for time scaling was used for the observations at the beginning or end of the time series. White noise was added to the sample time series of Eq. (14) by adding increasing levels of white noise, where w_{WN} scales the noise levels. Finally, biased noise was simulated by introducing biased observations in the sample time series of Eq. (14). This was done by replacing a number (w_{BN}) of the sample time series values by noise (biased low value of 0.1). This was done iteratively to generate several sample time series with an increasing number (w_{BN}) of noise values.

The amount of variability introduced in the MC simulations depends on the parameters w_{Asc} , w_{Ash} , w_{Tsc} , w_{Tsh} , w_{WN} , and w_{BN} , which were defined according to Table 3. These parameters span a wide variety of levels of introduced variability and allow to understand the effect of different levels on D_s performance. The difference in w_{Ash} and w_{WN} for the NDVI, EVI and LAI data results from the observed data value intervals of both data sets (i.e., most observed values in [0, 1] interval for NDVI and EVI vs. [0, 5] interval for LAI) to obtain similar effects for similar scaling parameters.

3.5. Sensitivity analysis

The MC simulations allow to quantitatively assess the effect of w_{Asc} , w_{Ash} , w_{Tsc} , w_{Tsh} , w_{WN} , and w_{BN} on the different D_s . This was done by calculating each D between (i) 500 sample time series of each LC type from the MC simulations of Eqs. (15–20) and (ii) the corresponding LC mean time series ($\bar{f}^{LC}(t)$). The retrieved D were subsequently compared with the corresponding intra-class distance D_{IC} by calculating D/D_{IC} . D_{IC} represents the natural intra-class variability of within class distances and is obtained by calculating each D between (i) 500 sample time series of each LC type from the

Table 2
Equations for different Monte Carlo simulations.

Effect	Equation	Parameters
Amplitude scaling	$f^{LC}(t) = (\bar{f}^{LC}(t) + \alpha \sigma^{LC}(t)) * \beta$ (15)	$\beta =$ pseudo-random value from normal distribution $N(\mu=1, \sigma=w_{Asc})$
Amplitude translation	$f^{LC}(t) = (\bar{f}^{LC}(t) + \alpha \sigma^{LC}(t)) + \beta$ (16)	$\beta =$ pseudo-random value from normal distribution $N(\mu=0, \sigma=w_{Ash})$
Time scaling	$f^{LC}(t) = \bar{f}^{LC}(t') + \alpha \sigma^{LC}(t')$ (17)	$t' =$ randomly elongated or shortened (with β observations) time series. $\beta =$ pseudo-random value from discrete uniform distribution ($-w_{Tsc} < \beta < w_{Tsc}$)
Time translation	$f^{LC}(t) = \bar{f}^{LC}(t + \beta) + \alpha \sigma^{LC}(t + \beta)$ (18)	$\beta =$ value that differs in time by a pseudo-random value from normal distribution $N(\mu=0, \sigma=w_{WN})$
White noise	$f^{LC}(t) = \bar{f}^{LC}(t) + \alpha \sigma^{LC}(t) + \beta(t)$ (19)	$\beta(t) =$ pseudo-random value from normal distribution $N(\mu=0, \sigma=w_{WN})$
Biased noise	$f^{LC}(t) = \bar{f}^{LC}(t') + \alpha \sigma^{LC}(t)$ (20)	$t' =$ time series that consists of the original time series of Eq. (14) with a number (w_{BN}) of observations replaced by noise (biased low value of 0.1).

Table 3
Parameter setting for the different Monte Carlo simulations.

	NDVI and EVI	LAI
Amplitude scaling	$w_{Asc} = 0.02, 0.04, \dots, 0.2$	$w_{Asc} = 0.02, 0.04, \dots, 0.2$
Amplitude translation	$w_{Ash} = 0.01, 0.02, \dots, 0.1$	$w_{Ash} = 0.01, 0.02, \dots, 0.1$
Time scaling	$w_{Tsc} = 1, 2, \dots, 10$	$w_{Tsc} = 2, 4, \dots, 20$
Time translation	$w_{Tsh} = 1, 2, \dots, 10$	$w_{Tsh} = 2, 4, \dots, 20$
White noise	$w_{WN} = 0.01, 0.03, \dots, 0.19$	$w_{WN} = 0.05, 0.15, \dots, 0.95$
Biased noise	$w_{BN} = 1, 2, \dots, 10$	$w_{BN} = 1, 2, \dots, 10$

MC simulations in Eq. (14) and (ii) the corresponding LC mean time series ($f_{LC}^{MC}(t)$).

Since D/D_{IC} compares the introduced effects (D) with the standard variability (D_{IC}), it quantifies the magnitude of the introduced effects relative to the intra-class variability. As a result, it allows to intercompare the different D s. This is more complicated when analyzing absolute D values as they are defined on different scales. Moreover, it implies that D/D_{IC} should be interpreted relative to the parameters settings in Table 3 in combination with the intra-class variability in LC time series.

4. Results

All subsequent figures represent the mean outcome of the annual analyses repeated in the 2001–2006 time interval. The choice to represent the results by the mean outcome was driven by clarity purposes and the small inter-annual variability between annual analyses.

4.1. Time series properties

Fig. 4 shows the basic time series statistics (i.e., mean and variance over time, serial correlation) of the NDVI, EVI, and LAI time series. For the mean time series it can be seen that, conform to Fig. 3, NDVI and EVI time series show similar behavior, but that NDVI covers a wider range than EVI. Furthermore, the LAI time series are not confined in the $[-1, 1]$ interval and show more abrupt changes at the beginning and the end of the growing season.

The variance of the time series data indicates that NDVI and EVI demonstrate a low intra-class variance (IC), but a much higher inter-class variance. Moreover, a timing difference in inter-class variance can be noticed between the NDVI and EVI data: the highest inter-class variance appears outside the growing season for the NDVI and within the growing season for the EVI data. This difference can be explained by the sensitivity of NDVI and EVI to background reflectance. Since the EVI is designed to be de-coupled of the canopy background reflectance (Huete et al., 2002), it will not capture the variance due to background reflectance, especially important outside of the growing season. The variance of LAI data, on the other hand, shows a clear seasonality, both in intra- and inter-class variance.

Comparison of the serial correlation reveals the difference in temporal resolution for the NDVI, EVI (both 16 day) and LAI (8 day) data, where the serial correlation decreases slower for LAI than for NDVI and EVI due to the higher temporal resolution of the LAI data. Additionally, it shows that the difference in serial correlation between NDVI–EVI and LAI data is due to the observation interval, as similar serial correlations are obtained for identical time lags (i.e., lag in function of time, not in function of observation). For example, the serial correlation at a lag of ten observations (i.e., a time lag of $10 \times 8 = 80$ days) corresponds to the serial correlation at a lag of five NDVI and EVI observations (i.e., a time lag of $5 \times 16 = 80$ days). This illustrates again serial correlation is driven by the seasonal cycle of phenological variability (Zoffoli et al., 2008), but may show up differently due to the temporal resolution of the data.

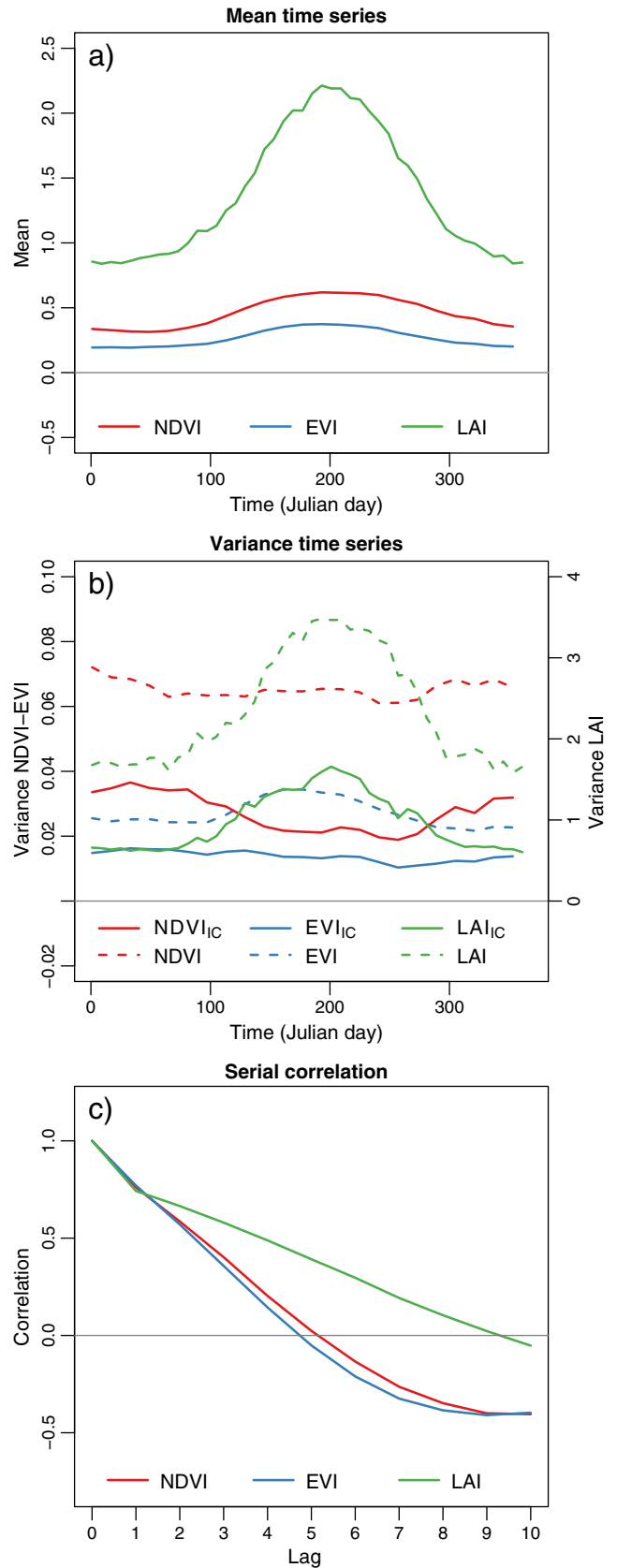


Fig. 4. Illustration of basic time series statistics of NDVI, EVI, and LAI data used in the MC simulations: a) mean in function of time; b) intra-class (IC) variance and inter-class variance in function of time; and c) serial correlation in function of lag in observations, where one observation represents a time lag of 16 (NDVI and EVI) and 8 days, respectively.

4.2. Monte Carlo simulation

Figs. 5–7 illustrate the effect of a) amplitude scaling, b) amplitude translation, c) time scaling, d) time translation, e) white noise, and f) biased noise on the D/D_{IC} values for the NDVI, EVI, and LAI time series respectively. Based on the change of each similarity measure D in function of w_{Asc} , w_{Ash} , w_{Tsc} , w_{Tsh} , w_{WN} , and w_{BN} , the sensitivity of each D can be determined as large changes in D/D_{IC} indicate high sensitivity.

Generally, the introduced amplitude effects (i.e., amplitude scaling and translation) result in smaller changes in D/D_{IC} values than time scaling, time translation or noise effects. This difference between amplitude and timing-noise effects, however, is mainly the result of the parameter settings in Table 3, which should be interpreted relatively to the existent intra-class variability. Consequently, higher values of w_{Asc} or w_{Ash} relative to the intra-class variability will result in higher sensitivities.

Comparison of the D s shows that different responses to the induced effects can be distinguished. Firstly, the Minkowski metrics D_{Man} and D_E are sensitive to all introduced changes in w_{Asc} , w_{Ash} , w_{Tsc} , w_{Tsh} , w_{WN} , and w_{BN} , where D_{Man}/D_{IC} values exhibit an almost linear increase for all introduced changes and D_E/D_{IC} shows a higher, often non-linear sensitivity. This higher sensitivity can be explained by D_E 's non-linear character and responsiveness to outlier values.

Secondly, the PCA based distance D_{PCA} performs very similar to D_{Man} for amplitude and timing effects, whereas it shows a reduced sensitivity when noise is introduced.

Thirdly, the Fourier based D_{Fk} displays also an almost linear increase for all introduced changes. Consequently, it resembles D_{Man} with a similar sensitivity to amplitude scaling, a lower sensitivity to amplitude translation, and a higher sensitivity to time scaling. For the NDVI and EVI data, D_{Fk} shows a higher sensitivity to noise than D_{Man} , but for the LAI data it is opposite.

Fourthly, the Mahalanobis distance D_{Mah} shows the largest absolute sensitivity to all introduced changes (Note: the D_{Mah} shown in Figs. 5–7 is represented on a logarithmic scale). Relatively, however, this sensitivity is especially strong when large deviations from the intra-class variability are introduced by the MC simulations. These large deviations from the intra-class variability occur, for example, when time scaling and time translation effects are introduced that cause large changes in the periods of green-up and dormancy which differ strongly from the intra-class variability. It also explains the difference in sensitivity of the NDVI, EVI, and LAI data sets to changes in w_{Ash} and w_{BN} , as these data sets show clear differences in intra-class variability (Fig. 4b). For example, the LAI time series are strongly non-stationary with a lower intra-class variance outside the growing season (Fig. 4b). Consequently, D_{Mah} will give extra weight to the changes introduced outside the growing season and less weight to the introduced changes within the growing season. Since amplitude translation relatively has a more pronounced effect outside the growing season and biased noise relatively has a stronger effect within the growing season, D_{Mah} shows an increased sensitivity to w_{Ash} and decreased sensitivity to w_{BN} for the LAI data. The NDVI and EVI data, on the other hand, show a stable intra-class variance and will therefore account equally for the amplitude shift and biased noise changes. However, as the absolute effect of biased noise is much stronger than the effect of small amplitude shift changes, NDVI and EVI data show a larger sensitivity to w_{BN} than to w_{Ash} .

Fifthly, the Pearson's cross-correlation coefficient displays the expected unchanged D_{CC} values when amplitude effects are inserted. However, when time scaling, time translation or noise effects are introduced it results in almost linear increases in $2 - D_{CC}$ and thus a linear decrease in D_{CC} .

Sixthly, the Fourier based similarity measures D_{FFT} , D_ξ differ from the other D as they demonstrate specific sensitivities. D_ξ , for example,

is very sensitive to time scaling effects (i.e., very steep increase of D_ξ with D_{Tsc}), less sensitive to time translation, and insensitive to amplitude effects. D_{FFT} , on the other hand, shows a large sensitivity to time scaling and translation (especially for the NDVI and EVI data) and is less affected by amplitude effects. Both D_{FFT} and D_ξ show moreover a high sensitivity to noise effects, although they were designed based on the assumption that noise was eliminated by taking adequate FT components.

5. Discussion

5.1. Performance of similarity measures

Based on the results, it can be seen that most D values increase when the original time series are affected by changes in amplitude, timing effects, or noise. However, the sensitivity to these changes is not similar between all D s and four main groups of similarity measures with different sensitivities can be distinguished: (i) the Minkowski metrics (D_{Man} , D_E), PCA based (D_{PCA}), and F_k -distance criterion (D_{Fk}), (ii) the Mahalanobis distance that accounts for temporal correlation and non-stationarity of variance, (iii) Pearson's cross-correlation D_{CC} that accounts for temporal correlation, and (iv) the Fourier based measures (D_{FFT} , D_ξ).

In the first group D_{Man} , D_E , D_{PCA} , D_{Fk} show similar behaviors with subtle distinctive features. The similar behavior between these four measures can be explained by the fact that they all are difference measures that quantify the difference in time series values, whereas the distinctive features are the result of their specific characteristics. For example, D_{Man} and D_E quantify the difference in raw data values (see Eq. (1)), but D_E is more sensitive to outlier values due to its non-linear character.

D_{PCA} is also a difference measure as the PCA transforms the data to a new coordinate system based on a linear transformation, and D_{PCA} uses the difference of these PCs. Mathematically, D_{PCA} is even identical to D_E when all PCs are included. Consequently, the differences between D_{PCA} and D_E are the result of reducing the number of PCs. Due to the dimensionality reduction in this study, D_{PCA} is less sensitive to noise effects, since parts of the noise is expressed in the later PCs that do not describe the majority of the total variance in the data set and are not included in D_{PCA} . Amplitude and timing effects, on the other hand, are clearly captured by the first three PCs, resulting in higher sensitivities. Nevertheless, the sensitivity of D_{PCA} is still lower than for D_E , but this can be explained by the dimensionality reduction, since part of the variability due to the introduced effects is captured by later PCs and thus not quantified. This stresses the importance of a proper understanding of the captured variability (e.g., amplitude, timing, noise effects) in the m selected PCs, as it will determine the sensitivity to these effects.

Finally, D_{Fk} is also a difference measure, as it is based on the Fourier transform of the difference between raw data values of two time series (Lhermitte et al., 2008). Since the FT components were used that express the majority of the ecosystem periodic variability, the similarity between D_{Fk} and the other difference measures is logical. However, as D_{Fk} uses the FT of the difference, it is specifically sensitive to differences that result in high $A_k^p - q$. This occurs, for example, as a result of time scaling or time translation.

The second group consists of D_{Mah} that measures the difference between time series, but that also accounts for the temporal cross-correlations in the data set and non-stationarity of variance. As a result, it is specifically sensitive towards changes that create large deviations from the intra-class variability (e.g., the effect of amplitude shift on LAI data outside the growing season) or from the temporal cross-correlations in the data set (e.g., time scaling, time translation or white noise).

The third group consists of D_{CC} that quantifies the temporal cross-correlation and does not account for the difference between time

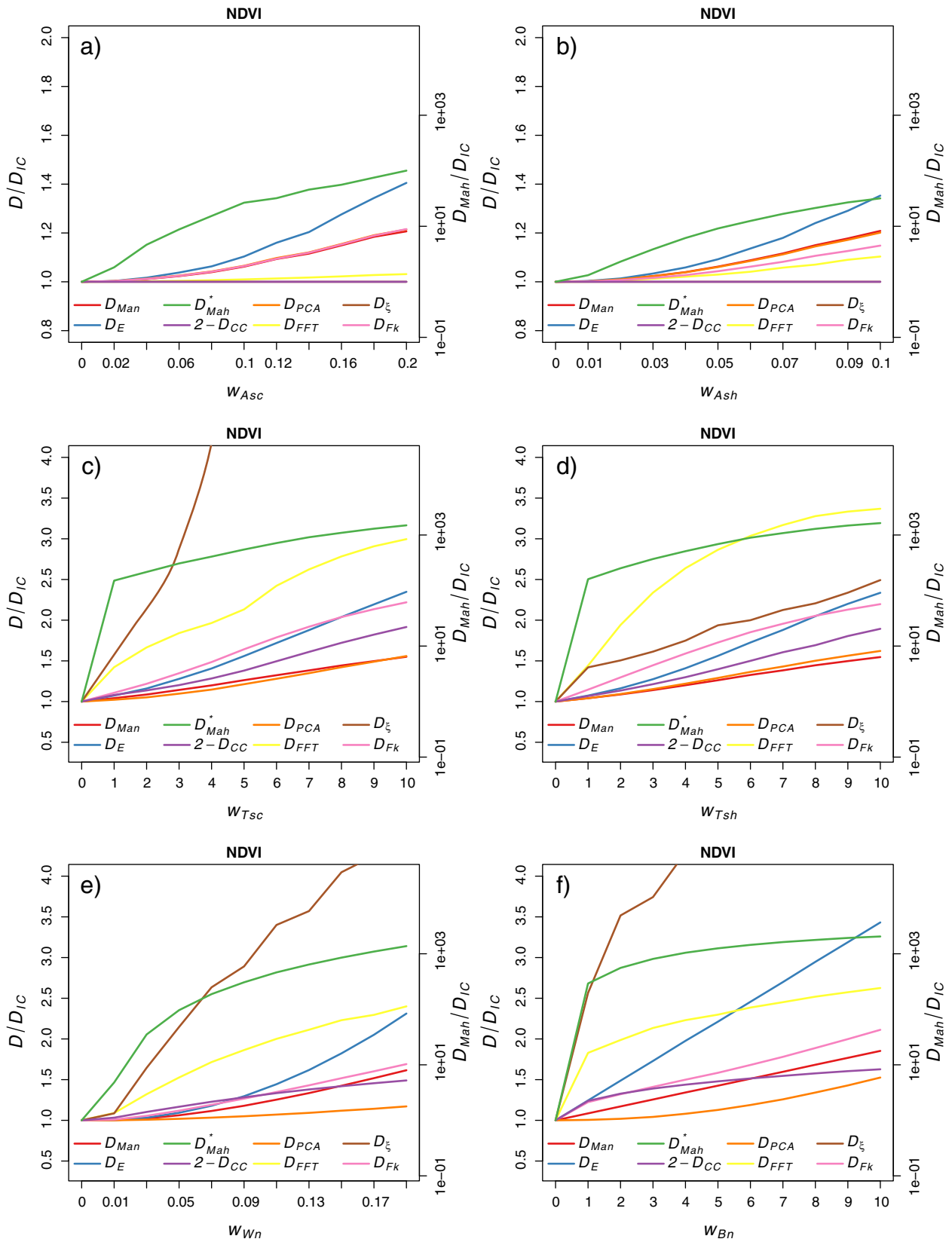


Fig. 5. Illustration of the effect of a) amplitude scaling, b) amplitude translation, c) time scaling, d) time translation, e) white noise, and f) biased noise on the D/D_{IC} values for the NDVI time series time series. Note that D_{CC} has been adjusted to $2 - D_{CC}$ to be represented on the same data interval as the other D . This implies that $2 - D_{CC} = 0$, when perfect correlation ($D_{CC} = 1$), and $2 - D_{CC}$ increases when the correlation decreases. Note moreover, the * with D_{Mah} to highlight that D_{Mah}/D_{IC} is represented by the logarithmic scale on the right side of each graph.

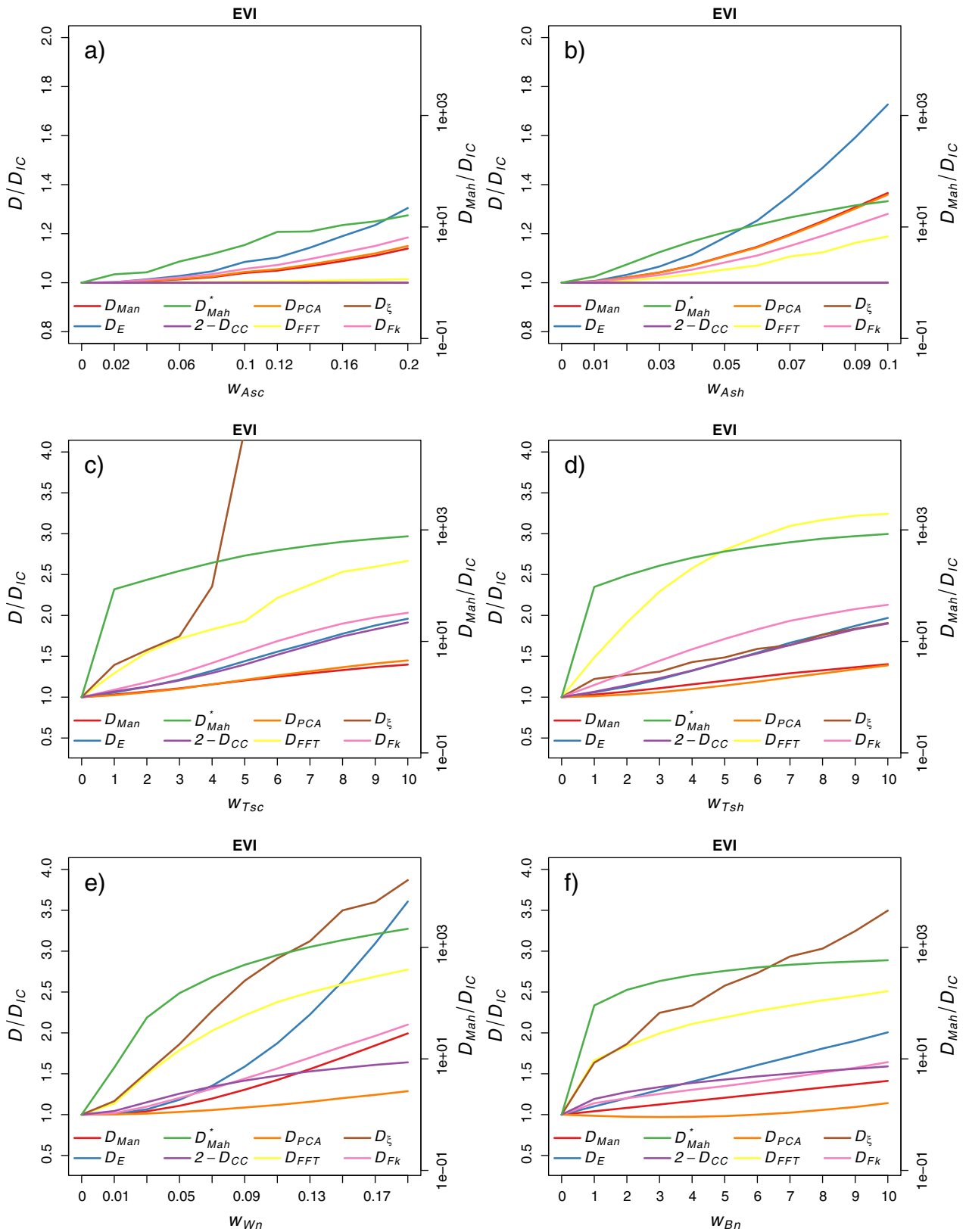


Fig. 6. Illustration of the effect of a) amplitude scaling, b) amplitude translation, c) time scaling, d) time translation, e) white noise, and f) biased noise on the D/D_{IC} values for the EVI time series. Note that D_{CC} has been adjusted to $2 - D_{CC}$ to be represented on the same data interval as the other D . This implies that $2 - D_{CC} = 0$, when perfect correlation ($D_{CC} = 1$), and $2 - D_{CC}$ increases when the correlation decreases. Note moreover, the * with D_{Mah} to highlight that D_{Mah}/D_{IC} is represented by the logarithmic scale on the right side of each graph.

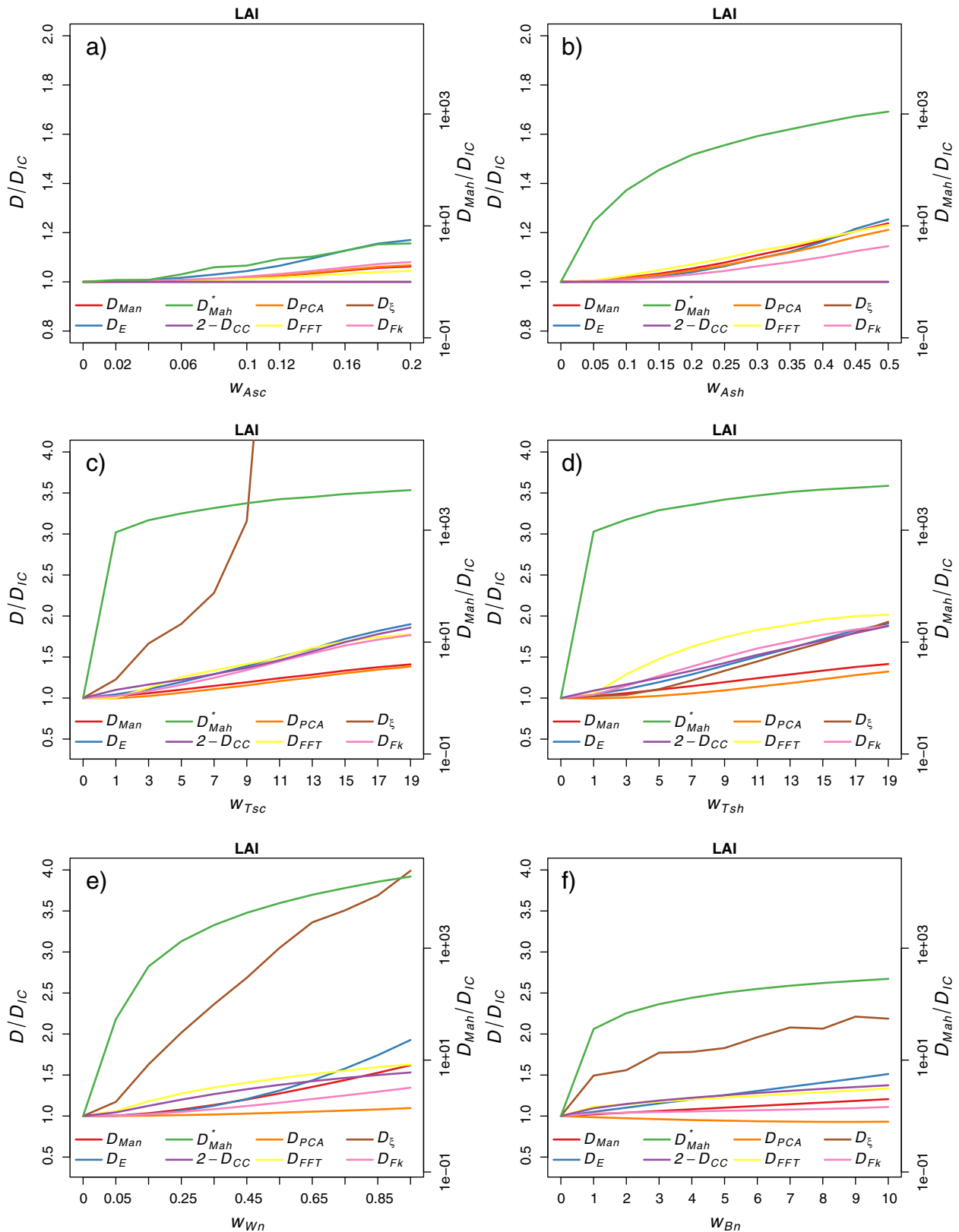


Fig. 7. Illustration of the effect of a) amplitude scaling, b) amplitude translation, c) time scaling, d) time translation, e) white noise, and f) biased noise on the D/D_{IC} values for the LAI time series. Note that D_{CC} has been adjusted to $2 - D_{CC}$ to be represented on the same data interval as the other D . This implies that $2 - D_{CC} = 0$, when perfect correlation ($D_{CC} = 1$), and $2 - D_{CC}$ increases when the correlation decreases. Note moreover, the * with D_{Mah} to highlight that D_{Mah}/D_{IC} is represented by the logarithmic scale on the right side of each graph.

series. It is not affected by amplitude effects as they do not affect the correlation, but it is highly sensitive to time scaling, time translation and noise effects. Both time translation and time scaling create a lag

between the original and simulated time series values. Consequently, the effect of that lag on the correlation can be understood by looking at the serial correlation at different lags (Fig. 4c), which indicates a

decrease in correlation for increasing lags. The noise, on the other hand, also results in a decrease correlation, as also shown by Evrendilek and Gulbeyaz (2008).

The fourth group consist of the Fourier based measures (D_{FFT} , D_{ξ}) with specific sensitivities. They are completely (D_{ξ}) or relatively (D_{FFT}) robust to amplitude effects, but highly sensitive to time translation and scaling, and much more sensitive to noise effects than assumed by Moody and Johnson (2001), Evans and Geerken (2006), and Wagenseil and Samimi (2006). For D_{FFT} , the high sensitivity to time effects and relative robustness to amplitude effects can be explained by the equal weights for amplitude and phase in Eq. (8). This equation will be dominated by phase differences between time series, since phase values differ from $-\pi$ and π , while the amplitudes for NDVI–EVI time series only vary between 0 and 1. This is also apparent in the study of Wagenseil and Samimi (2006), where the variability in phase values is much higher than for the amplitude values. As a result, D_{FFT} is not affected by small changes in amplitude values due to w_{Asc} and w_{Ash} , whereas small changes in phase values due to time translation result in a abrupt increase. For the LAI time series, on the other hand, this dominance of phase differences is not as strong, since LAI values vary between 0 and ± 5 . For D_{ξ} , on the other hand, the robustness to amplitude effects can be explained by its design, whereas the effect of time scaling on D_{ξ} can be attributed to its defined sensitivity to shape changes, which resemble time scaling. Although the effect of time translation is unexpected given D_{ξ} s design (Evans & Geerken, 2006), it can be explained by looking at the differences between time translation in theory and in reality. In the theoretic definition of time translation, the observation value that disappears on the right, reappears on the left (or vice versa). In real ecosystems, however, the observations at the beginning and end of the time window do not necessarily correspond and may cause changes the individual FT components and consequently in D_{ξ} .

The high sensitivity of D_{FFT} and D_{ξ} to noise effects stresses the importance of a proper selection of FT components, as it can be explained by the decomposition of noise in simpler periodic signals. In this context, D_{FFT} and D_{ξ} were defined robust to noise based on the assumption that noise is only contained in the high frequency Fourier components. This assumption, however, is not true for white noise and biased noise. White noise has equal power in any frequency component (Vasseur & Yodzis, 2004) and it tends to influence the similarity measures when the power of the noise equals the time series signal power. This influence can be understood by using the additive property of Fourier transform, which explains how noise components with relative high power result in arbitrary similarity for D_{FFT} and D_{Fk} (see Appendix A).

The effect of biased noise on D_{FFT} and D_{ξ} is comparable since biased low or high values also result in high power in the first Fourier components. This is illustrated in Fig. 8, where Fig. 8a shows the original NDVI, EVI, and LAI time series of one LC class, white noise and biased noise, and Fig. 8b displays amplitude of the first ten Fourier components. Comparison of these Fourier components in Fig. 8b shows that A_k^p still contains a high signal to noise ratio (SNR) for $k=1$, but that the SNR is very low and even below one for $k=2$. Consequently, the noise for $k=2$ will influence the similarity measures D_{FFT} and D_{ξ} , resulting in high sensitivities for increased noise effects. This sensitivity is specifically strong for the biased noise in the NDVI time series, as it introduces relatively high power in the first A_k^p components. For the LAI data, on the other hand, the effect of the introduced biased noise on A_1^p and A_2^p is less pronounced as the SNR is higher, resulting in smaller increases in D_{FFT} and D_{ξ} for the LAI data. The sensitivity of D_{FFT} and D_{ξ} to noise effects stresses again the importance of selecting only FT components with a high SNR. In this context, the assumption that noise restricted to the high frequency components is, as shown, not necessarily true and thus the SNR needs to be considered when selecting the FT components.

Although noise also affects difference measure D_{Fk} , its effect is less pronounced. This can be explained by looking at Eq. (13), where D_{Fk} is

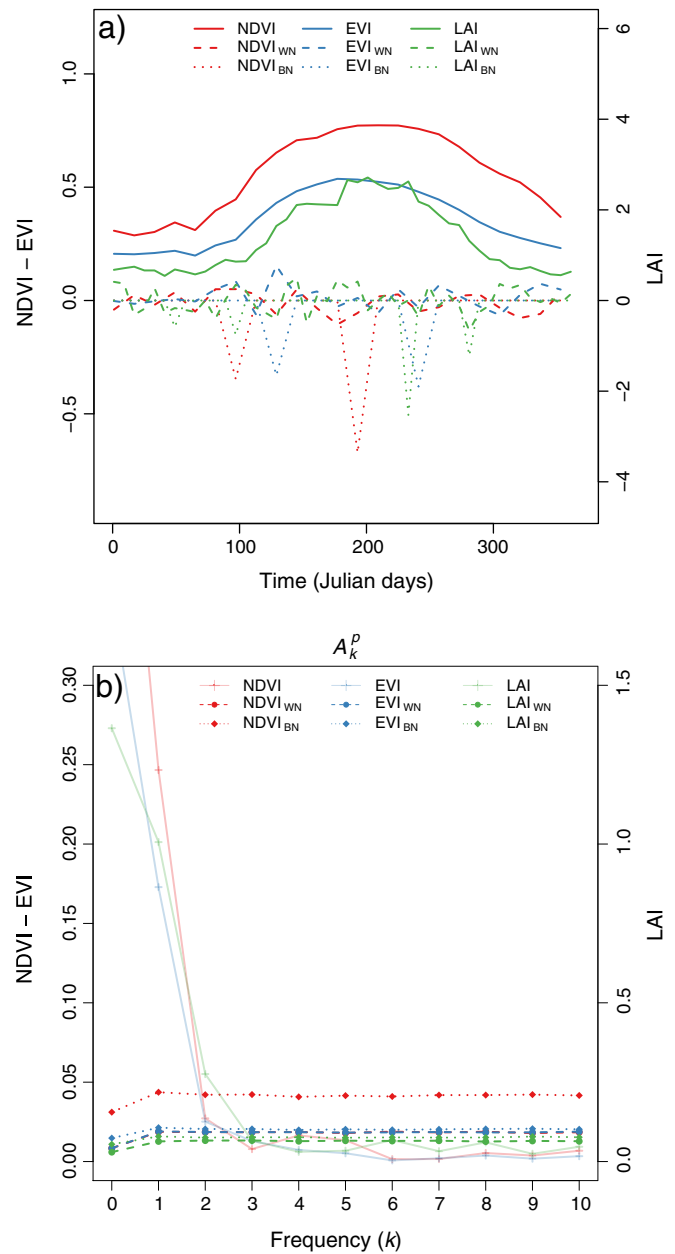


Fig. 8. Example of amplitude of noise in comparison with NDVI, EVI and LAI time series: a) NDVI, EVI, and LAI time series for a Cropland/Natural Mosaic pixel time series and noise time series ($w_{WN} = 0.05$ for NDVI–EVI and $w_{WN} = 0.25$ for LAI; $w_{BN} = 2$ for NDVI, EVI and LAI) in the additive approach; b) amplitude A_k^p of the first ten Fourier components of Cropland/Natural Mosaic pixel time series (NDVI, EVI and LAI) and the mean of the added noise components (WN; $w_{noise} = 0.05$ for NDVI–EVI and $w_{noise} = 0.25$ for LAI; BN; $w_{BN} = 2$ for NDVI, EVI and LAI).

dominated by the FT components with high information content. This implies that, although the power of A_2^{WN} and A_2^{BN} equals the power of A_2^p and A_2^q , they will only contribute little to the final D_{Fk} when A_2^{p-q} contains little power. This effect is not true for D_{FFT} where each phase and amplitude has equal weight on the outcome. Consequently, a low SNR in one component (e.g., A_2^p) will tend to dominate D_{FFT} , although the overall time series' SNR is not necessarily very low (e.g., when A_1^p has a high SNR and $A_1^p \gg A_2^p$). A similar conclusion was drawn by Mimmack et al. (2001), who discussed the use of standardized PC scores in similarity assessment, and encountered a dominance of noise when each component was given equal weight instead of the weight related to its information content.

5.2. Importance of knowledge of time series characteristics

The heterogeneity in sensitivity of each D stresses the importance of understanding the time series characteristics before applying any classification of change detection approach. This requires knowledge of the time series characteristics related to baseline, amplitude, timing, noise of the ecosystem time series and highlights the importance of preliminary data analysis to understand these. This is also shown in this quantitative comparison, where the different sensitivities of D for NDVI, EVI, and LAI can be explained by the temporal characteristics of each data set. Consequently, it implies that analysis of the individual time series and their descriptive statistics (i.e., mean/median and variance over time (Fig. 3), serial correlation (Fig. 4c)) is crucial before applying any classification or change detection approach, since it will give insight in the temporal data characteristics. For example, the mean time series allow an analysis of the phenological cycle and their differences over time. The variance over time, on the other hand, permits analysis of the temporal variability in amplitude and timing effects as (i) variability in amplitude translation affects the variance over time uniformly, (ii) variability in amplitude scaling increases the variance for the high value observations and (iii) variability in timing effects specifically alters the variance in the periods of green-up and dormancy.

For the transformation based similarity measures it also requires an analysis of the PCA or FT components before using the transformed time series. This analysis of PCA or FT components will explicate what temporal variability will be accounted for. Wagenseil and Samimi (2006), for example, stressed that the assumption of Fourier analysis (i.e., the data can be represented by a periodical and sinusoidal signal) is often not satisfied for the complex shape of NDVI signals, and may therefore require high frequency terms for suitable approximation. In this context, Lhermitte et al. (2008) analyzed the contribution of each FT component in the differenced time series signals in function of the spatial distance between pixels before applying D_{FK} . Similar analysis is essential before using D_{FFT} or D_{ϵ} , since it will provide comprehension of the relative contribution of amplitude and phase (e.g., understanding the contribution of amplitude and phase values in Eq. (8)) and avoid hidden dominance of either of both.

Additionally, noise estimation is a crucial step before applying time series similarity measures as it is crucial to distinguish signals from the background noise (Mann & Lees, 1996). Hird and McDermid (2009) in this context warned time series data users to consider both their ultimate objective and the nature of the noise present in an NDVI data set when selecting an approach to noise reduction. In this framework, a number of interesting methods have been proposed that allow separation of noise from the smoothed phenology signals based on several fitting (Bradley et al., 2007; Carrao et al., 2010; Chen et al., 2004; Hermance et al., 2007; Jönsson & Eklundh, 2004; Ma & Veroustraete, 2006; Roerink et al., 2000) or decomposition methodologies (Cihlar et al., 1997; Lu et al., 2007; Verbesselt et al., 2010a) that sometimes also handle intervals of missing values. Since these methodologies subsequently allow to quantify the signal to noise ratio (Bacour et al., 2006; Carrao et al., 2010; Dash et al., 2008; Evrendilek & Gulbeyaz, 2008; Geerken et al., 2005b) and determine the statistical properties of the noise (e.g., noise color; Vasseur & Yodzis, 2004), they also allow to determine the influence of noise on the D .

Besides, the effect of length of the time series and serial correlation should seriously be considered when assessing time series similarity. In our analysis, the serial correlation analysis indicates that NDVI, EVI and LAI time series show high serial correlation for short observation intervals (Fig. 4c); especially for the LAI data set with 8-day observation composites vs. 16-day composites for NDVI and EVI. As a consequence, the subsequent observations in the time series contain redundant information, certainly when the evolution of vegetation at various phenological stages is relatively slow and not related to abrupt

disturbances such as fire, frost, or harvesting. In classification approaches this redundant information may result in high accuracies with few observations as demonstrated by Carrao et al. (2008), who found a sharp increase in classification accuracy for few observation dates followed by small increases with more observation dates. Although, the best performance was attained by combining all dates, the classification accuracy reached already an acceptable rate with only a few input dates. Nevertheless, fine time scale variations are not accounted when using fewer temporal inputs (Lambin, 1996) and may complicate phenological event detection (Zhang et al., 2009). This was also shown by Lhermitte et al. (2011) and Veraverbeke et al. (2010) who stressed the importance of high frequent observations to capture the intra-annual changes due to abrupt disturbances. Analysis of the serial correlation as performed by Alexandridis et al. (2008) is therefore essential to determine an appropriate temporal sampling interval for monitoring vegetation. This is certainly essential when the cross-correlation similarity between time series is considered, as Olden and Neff (2001) stressed that serial correlation can inflate estimates of cross correlation.

5.3. Importance of ecosystem dynamics and knowledge of time series variability

Besides understanding the time series data characteristics, the definition of the ecosystem dynamics one want to discriminate is also crucial in the appropriate selection of D . This choice of ecosystem dynamics should be driven by the ability to account for variability at one scale, while identifying differences at another (Verbesselt et al., 2010a; Verbesselt et al., 2010b). For example, in classification approaches of ecosystem dynamics, one may be interested, depending on the application, in using similarity measures which are specifically sensitive or insensitive to the soil background, understory vegetation, etc.. In change detection approaches, on the other hand, one may want to discriminate changes in vegetation type, without considering phenological changes (e.g., onset and timing of phenological events; Evans & Geerken, 2006) or vice versa (de Beurs & Henebry, 2005).

Before defining the ecosystem dynamics to discriminate the understanding of the data variability is crucial. In this context, an analysis of the natural versus changed variability (for change detection approaches) or intra- versus inter-class variability (for classification approaches), can provide insights in the dynamics and separability. This can be done by calculating the overall data variability and trying to understand the causes of variability (e.g., Julien & Sobrino, 2008; Linderman et al., 2005) or by using pre-determined groups or classes and compare their intra- versus inter-class variability. Alternatively, statistics that express the separability between groups or classes such as the simple index (Somers et al., 2009; Zhang et al., 2006), the Jeffries–Matusita distance (Lu & Weng, 2007) or Mahalanobis distance (Carrao et al., 2008) might serve as an quantitative indicator of separability. Based on these approaches, the D that maximizes the desired separability can be selected, for example by comparing these using D/D_{IC} . Generally, this selection is a combination of ultimate objective and the nature of the separability. For example, amplitude sensitive difference measures might be optimal, when amplitude differences determine the separability of changed–unchanged or different classes (e.g. difference between grass land and forest types; Lu et al., 2003), whereas correlation based D s might be better when the separability is determined by correlation.

6. Case study

As an illustration of the importance of understanding the time series characteristics related to baseline, amplitude, timing, noise and their intra- and interclass variability, this sections present a case study based on LC classification using NDVI, EVI and LAI time series. The goal of this

case study was not to determine the optimal LC classification approach, but to demonstrate the importance of understanding the time series data and their variability as it may affect the performance of each D .

6.1. Methodology

For the LC classification, 500 sample NDVI, EVI, and LAI time series (2001–2006) per LC type were randomly extracted from the n_{LC} NDVI, EVI and LAI time series for the northern hemisphere (Section 3.1).

Before classifying these time series, we aimed at understanding the time series characteristics related to baseline, amplitude, timing, noise of the ecosystem time series. The aspects related to baseline, amplitude, timing are already illustrated in Figs. 3–4 and discussed in Sections 3.1–4.1. To understand the importance of noise on the time series, the Timesat program was selected to produce temporally smooth estimates of NDVI, EVI and LAI (Jönsson & Eklundh, 2004). The iterative and adaptive Savitzky–Golay (SG) filtering method was selected, since it has been shown to be most effective to minimize overall noise (Hird & McDermid, 2009). Before applying the SG filter, spurious observations were identified using the data quality control flags and assigned weights for the SG filter ($w=1$ for good quality observations; $w=0.5$ for marginal data; $w=0$ for cloudy data and fill values). Subsequently, the SG filter was applied using two fitting iterations, a window width of three months and an adaptation strength of two. These optimal fitting settings were selected after visual inspection. The result of the Timesat fitting process can be seen in Fig. 9 which displays the raw and fitted time series for a Deciduous Broadleaf Forest pixel. For this pixel it is apparent that the 8-day LAI time series contains more noise than the 16-day NDVI–EVI time series. This is also visible when looking at the FT amplitudes for components A_k of all raw and Timesat fitted time series in Fig. 10, where the noise time series (i.e., raw time series minus Timesat fitted time series) contains relatively higher amplitude levels for the LAI data than for the NDVI–EVI data. It also illustrates the relative importance of noise for A_k when $k>1$, where A_k contains similar amplitude values for the noise as for the Timesat fitted NDVI, EVI and LAI time series. This implies a low signal to noise ratio, which may interfere with A_k as discussed in Section 5.

The 500 sample time series of each LC type were subsequently classified by comparing the pixel’s annual time series with the mean annual time series of each LC type $\bar{f}^{LC}(t)$ and assigning the pixel to the most similar class in a minimum distance classification approach. Practically, this means pixel p ’s 2000–2001 time series is compared with each 2000–2001 $\bar{f}^{LC}(t)$ and assigned to the most similar LC. Afterwards, this process is repeated for 2001–2002, etc. This whole process was performed for both the raw and Timesat fitted time series.

The eight D s of Section 3.3 were used in the minimum distance classification. Additionally, alternative D_{FFT}^* , D_{ξ}^* , and D_{Fk}^* were calculated

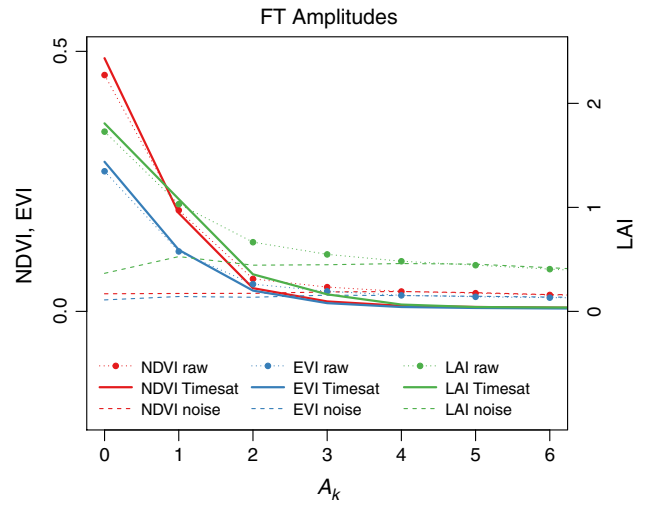


Fig. 10. Mean FT amplitudes for components F_k of the raw, Timesat fitted, and extracted noise time series.

which include only the mean and annual component ($k=0, 1$; $w_k=0.5$). The comparison of these alternative D_{FFT}^* , D_{ξ}^* , and D_{Fk}^* with D_{FFT} , D_{ξ} , and D_{Fk} allows to assess the importance of the noise for F_k ; $k>1$.

After the classification, overall accuracy across all classes was calculated as a measure of classification accuracy. Although this measure has been criticized as measure of accuracy (Foody, 2002; Strahler et al., 2006), it is a well established community protocol for classification accuracy and allows to compare the performance of the D s in a supervised classification approach (i.e., the class mean time series for each class are known).

6.2. Results and discussion

Fig. 11 illustrates the effect of each D on the overall classification accuracy in a minimum distance classifier. For all D , classification accuracies below 0.5 are obtained, whereas Herold et al. (2008) and Friedl et al. (2010) obtained in their validation of the MOD12 product overall accuracies across all classes of 78.3% and 74.8% respectively. The lower accuracies in this case study, however, are not unlogical as the original MOD12 LC classification is based on a more sophisticated ensemble supervised classification algorithm. The ensemble algorithm uses a combination of input time series products in a complex decision tree and artificial neural network classification algorithm to assign land cover classes using training data (Friedl et al., 2010). Additionally, the MOD12 product is post-processed to correct

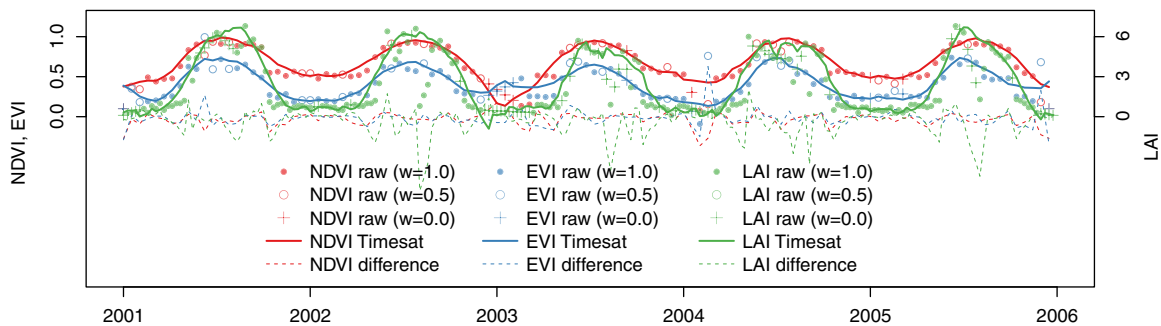


Fig. 9. Illustration of the Timesat Savitzky–Golay (SG) filtering method for a NDVI, EVI, and LAI time series for a Deciduous Broadleaf Forest pixel time series. The points ($w=1$ for good quality observations, $w=0.5$ for marginal data and $w=0$ for cloudy data and fill values) represent the raw data values, whereas the line represents the temporally smoothed time series. The difference between both can be attributed due to noise effects.

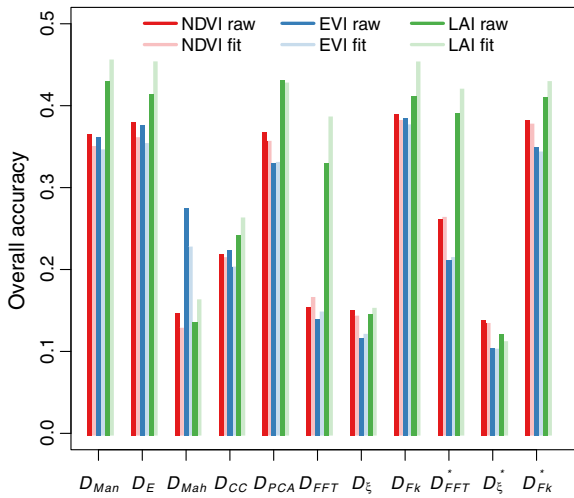


Fig. 11. Illustration of the overall classification accuracy when D is used in a minimum distance classifier approach. D_{Man} , D_E , D_{Mah} , D_{CC} , D_{PCA} , D_{FFT} , D_{ξ} , and D_{Fk} represent the Ds of Section 3.3 whereas D_{FFT}^* , D_{ξ}^* , and D_{Fk}^* were calculated using only the mean component and annual component ($k=0, 1$; $w_k=0.5$).

classification results for biases and to exploit geographic distribution information. In this case study, on the other hand, only one data set was used (NDVI, EVI and LAI respectively), the mean and standard deviation of $f^{LC}(t)$ were assumed to typify each LC type, and no post-processing or geographic corrections were applied. As a result, lower overall accuracies are not unlogical. However, as our goal was not to maximize absolute classification accuracy (e.g., by merging confusing classes in a post-classification approach), the relative accuracy still allows to determine the relative performance of each D and to understand the causes of this performance.

From the relative comparison of the Ds , it can be observed that similarity measures that quantify the difference between time series (D_{Man} , D_E , D_{PCA} , D_{Fk}) result in the highest accuracies with subtle differences between each of them. Secondly, the similarity measures that account for correlation (D_{Mah} , D_{CC}) generate much lower accuracies, where only D_{Mah} results in accuracies above 20% for the EVI data. This higher accuracy of D_{Mah} for the EVI data is the result of the EVI intra- and inter-class variance time series illustrated in Fig. 4, where only EVI data shows a low intra-class variance (IC) and high inter-class variance during the growing season. Consequently, D_{Mah} for the EVI data will be specifically sensitive to inter-class differences within the growing season, resulting in higher accuracies than for the NDVI and LAI data that do not have this difference within the growing season. Thirdly, the D_{FFT} shows variable results with higher accuracies for the LAI data than for the NDVI and EVI data. This is due to the phase dominance for D_{FFT} , which is stronger for the NDVI and EVI data due to their lower amplitudes values. Comparison of D_{FFT} and D_{FFT}^* also shows that better classification results are obtained for D_{FFT}^* with only the mean and annual FT components. This can be explained by the equal weight for all components in Eq. (8), whereas Fig. 10 illustrates that the A_k values with $k > 1$ contain little information. As a result, D_{FFT} is influenced strongly by A_2 and θ_2 with a low SNR. This effect of including A_2 and θ_2 is not apparent for D_{Fk} . This can be explained by the fact that only pixels with a high A_2^{-q} , which corresponds to a higher SNR, will significantly contribute to D_{Fk} . Fourthly, D_{ξ} and D_{ξ}^* performs poorly for all data sets, which indicates that solely shape information, without accounting for baseline and amplitude effects, cannot explain all variation between LC types. This was also apparent in Fig. 3, where the clearest distinction between LC types can be made based on baseline-amplitude information and confirms the work of De Fries et al. (1998), Hansen et al. (2000), Canisius et al. (2007), and Xia et al. (2008) who established that baseline-amplitude information constitutes the basis of the decision tree to discriminate LC types.

Comparison of classification performance between NDVI, EVI, and LAI data shows in general that LAI data performs best. This can be explained by (i) looking at the intra- and inter-class variance in Fig. 4, where the relative difference between intra- and inter-class variance is high during the whole year for the LAI data in comparison with the NDVI and EVI data. This implies that the LAI time series are more separable in this case study.

Moreover, the difference in accuracy between the raw and Timesat fitted time series reveals the influence of noise on the time series. For example, the raw EVI and NDVI time series generally perform better than their fitted counterparts, whereas the opposite can be perceived for the LAI data where the fitted data perform better than the original raw data. This difference between EVI, NDVI and LAI data is the result of their different SNR and the balance between time series integrity maintenance and noise removal. In this context, Hird and McDermid (2009) demonstrated that the Timesat SG fitting method is optimal for noise reduction, but does not always maintain the integrity of the time series. Moreover, they illustrated that noise reduction can reduce the quality of the raw time series when noise levels are low. This is also what happens here, where the NDVI and EVI data contain low noise levels (Fig. 10). Consequently, the gain of removing noise in the NDVI and EVI time series cannot counterbalance the loss of integrity, except for D_{FFT} where the noise in A_2 strongly affects D_{FFT} . For the LAI data, on the other hand, the removal of the stronger noise component effectively compensates for the loss of integrity in the classification, except for D_{PCA} on LAI data where the use of PCs already succeeds in isolating the noise from the raw time series.

Together these results illustrate the importance of understanding of the time series' baseline, amplitude, timing, noise and intra- and interclass variability, as they demonstrate how the classification accuracy for each D is affected by these. In this case study, for example, the baseline-amplitude provides more information to properly classify each LC class than the information related to correlation or shape alone, whereas the LAI data show a higher intra-inter-class separability for each LC, but are also more affected by noise. As a consequence, the difference measures D_{Man} , D_E , D_{PCA} , and D_{Fk} outperform the other D , especially for the LAI data, but noise removal is also more crucial.

7. Conclusion

Since time series similarity measures D play an important role in several approaches to study ecosystem dynamics based on remote sensing time series, there is a strong need for a more comprehensive understanding concerning the existent similarity measures. These measures range from Minkowski (D_{Man} , and D_E) and Mahalanobis (D_{Mah}) distance measures, to correlation (D_{CC}), Principal Component Analysis (PCA; D_{PCA}) and Fourier based (D_{FFT} , D_{ξ} , D_{Fk}) similarities. This understanding is specifically important since many of these similarity measures serve as underlying decision criterion in several time series clustering and change detection techniques and choice of the similarity may affect the final classification and change detection outcome.

This study therefore focused on the quantitative comparison of the frequently used time series similarity measures D in function of varying time series and ecosystem characteristics, such as amplitude, timing and noise effects. This comparison by means of Monte-Carlo simulations based on subsets of global MODIS Normalized Difference Vegetation index (NDVI) and Enhanced Vegetation Index (EVI) and Leaf Area Index (LAI) data revealed four main groups of time series similarity measures with different sensitivities: (i) D_{Man} , D_E , D_{PCA} , and D_{Fk} quantify the difference between time series, (ii) D_{CC} assesses the temporal correlation between time series, (iii) D_{Mah} also quantifies the difference but specifically accounts for temporal correlation and non-stationarity of variance, iv) the Fourier based measures D_{FFT} and D_{ξ} quantify a derived similarity based on specific frequency components.

The first group of difference measures is sensitive to all introduced effects, but show relatively the highest sensitivity to amplitude effects. The similar behavior between these four measures can be explained by the fact that they all are difference measures that quantify the difference in time series values. Their distinctive features, on the other hand, are the result of their specific characteristics related to outliers (D_E), Principal Component selection (D_{PCA}), or differenced time series (D_{Fk}). The second (D_{Mah}) and third group (D_{CC}) are highly sensitive to variations that change the temporal cross-correlation between time series (e.g., time scaling or translation and noise effects), whereas the performance of D_{Mah} also depends strongly on the intra- and inter-class variability. The fourth group of Fourier based measures (D_{FFT} and D_ξ), finally, show their specific sensitivity based on the selected Fourier components, where the signal to noise ratio and the balance between amplitude and phase dominance is of crucial importance.

As a result of these different sensitivities, it is essential to understand the ecosystem dynamics and time series characteristics related to baseline, amplitude, timing, noise and variability before selecting a D . This was illustrated in the quantitative comparison, as the different sensitivities of D for NDVI, EVI, and LAI data were obtained which relate specifically to the temporal characteristics of each data set. Additionally, the importance of understanding the time series noise and intra- and interclass variability was demonstrated in a case study based on LC classification, where it was shown how the time series' baseline, amplitude, timing, noise and intra- and interclass variability affect the classification accuracy based on D . Future users of time series similarity measures therefore need to consider the relation between the (i) ecosystem dynamics to be classified/ecosystem changes to be detected and (ii) and the time series characteristics of the data to be used.

Acknowledgments

This work was performed in the framework of a research project on satellite remote sensing of terrestrial ecosystem dynamics, funded by the Belgian Science Policy Office (GLOVEG-VG/00/01; GLOVEX-SR/16/81; ECOSEG-SR/01/108). This work was funded by a Marie-Curie IRG fellowship within the European Community's Seventh Framework Program to Jan Verbesselt. The authors thank the reviewers for their constructive remarks and detailed comments that led to an improved version of the manuscript.

Appendix A

The additive property of Fourier transform implies that addition in one domain (e.g., time domain) corresponds to addition in the other domain (e.g., frequency domain) (Bracewell, 2000). The result of adding noise to the NDVI, EVI, or LAI times series can therefore be considered as adding the Fourier transform of the noise to the original Fourier transform of the NDVI, EVI or LAI signal. An example of this addition is given in Fig. 12. In this illustration, the effect of white noise is the displacement of the original Fourier components (p and q) to a new random point on the circle around the original point. The radius of the circle will depend on the energy of the noise signal ($\sqrt{(F_k^c)^2 + (F_k^s)^2} = A_k^{noise} \sim w_{noise}$) due to Parseval's relation (Bracewell, 2000). The displacement of points p and q results in new amplitude and phase values for each FT component. This new amplitude and phase will depend on the relative difference between original A_k^p and A_k^{noise} . When the original A_k^p is high, the effect of the noise will be small. However, when $A_k^p \leq A_k^{noise}$, the effect will be large, and the new amplitude and phase values will change the D_{FFT} and D_ξ results. For example, a complete random phase value is obtained when the original A_k^p is smaller than the noise level NL (e.g., NL_2 in Fig. 12). Due to the unstandardized use of phase values in Eq. (8), the random phase value will result in arbitrary similarity measure D_{FFT} , even

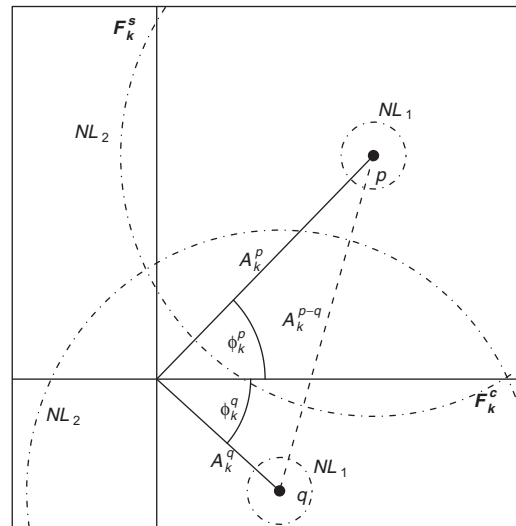


Fig. 12. Illustration of noise effects on Fourier components. F_k^c and F_k^s are amplitudes of the cosine and sine waves in rectangular notation, while A_k and ϕ_k are the amplitude and phase in polar notation, respectively. The introduction of random noise causes a displacement of the original p and q to new arbitrary points on the circle around p and q . The radius of this circle will depend on the noise level NL . Two different scenarios of noise levels are plotted to illustrate this effect (NL_1 and NL_2).

when $A_k^p \leq A_k^{WN}$ for only one k . The effect on Eq. (9) is of the same order as changes of A_k^p and ϕ_k^p will affect D_ξ and will transform it into an arbitrary distance measure, especially when the noise on A_1^p is exaggerated in further calculations of α_k and θ_k .

References

- Alexandridis, T. K., Gitas, I. Z., & Silleos, N. G. (2008). An estimation of the optimum temporal resolution for monitoring vegetation condition on a nationwide scale using MODIS/Terra data. *International Journal of Remote Sensing*, 29(12), 3589–3607.
- Anyamba, A., & Eastman, J. R. (1996). Interannual variability of NDVI over Africa and its relations to El Niño/Southern Oscillation. *International Journal of Remote Sensing*, 17(13), 2533–2548.
- Anyamba, A., Tucker, C. J., & Eastman, J. R. (2001). NDVI anomaly patterns over Africa during the 1997/98 ENSO warm event. *International Journal of Remote Sensing*, 21(10), 1847–1859.
- Azzali, S., & Menenti, M. (2000). Mapping vegetation–soil–climate complexes in southern Africa using temporal Fourier analysis of NOAA-AVHRR NDVI data. *International Journal of Remote Sensing*, 21(5), 973–996.
- Bacour, C., Breon, F. M., & Maignan, F. (2006). Normalization of the directional effects in noaa-avhrr reflectance measurements for an improved monitoring of vegetation cycles. *Remote Sensing of Environment*, 102(3–4), 402–413.
- Badeck, F.-W., Bondeau, A., Bottcher, K., Doktor, D., Lucht, W., Schaber, J., & Sitch, S. (2004). Responses of spring phenology to climate change. *The New Phytologist*, 162(2), 295–309.
- Bannari, A., Morin, D., Bonn, F., & Huete, A. R. (1995). A review of vegetation indices. *Remote Sensing Reviews*, 13(1), 95–120.
- Bayarjargal, Y., Karnieli, A., Bayasgalan, M., Khudulmur, S., Gandush, C., & Tucker, C. J. (2006). A comparative study of NOAA-AVHRR derived drought indices using change vector analysis. *International Journal of Remote Sensing*, 105(1), 9–22.
- Beck, P. S. A., Atzberger, C., Høgda, K. A., Johansen, B., & Skidmore, A. K. (2006). Improved monitoring of vegetation dynamics at very high latitudes: A new method using MODIS NDVI. *Remote Sensing of Environment*, 100(3), 321–334.
- Bence, J. R. (1995). Analysis of short time series: correcting for autocorrelation. *Ecology*, 76(2), 628–639.
- Benedetti, R., Rossini, P., & Taddei, R. (1994). Vegetation classification in the Middle Mediterranean area by satellite data. *International Journal of Remote Sensing*, 13(3), 583–596.
- Bergen, K. M., Brown, D. G., Rutherford, J. F., & Gustafson, E. J. (2005). Change detection with heterogeneous data using ecoregional stratification, statistical summaries and a land allocation algorithm. *Remote Sensing of Environment*, 97(4), 434–446.
- Bontemps, S., Bogaert, P., Titeux, N., & Defourny, P. (2008). An object-based change detection method accounting for temporal dependences in time series with medium to coarse spatial resolution. *Remote Sensing of Environment*, 112(6), 3181–3191.
- Borak, J. S., Lambin, E. F., & Strahler, A. H. (2000). The use of temporal metrics for land cover change detection at coarse spatial scales. *International Journal of Remote Sensing*, 21(6–7), 1415–1432.

- Bracewell, R. N. (2000). *The Fourier transform and its applications* (Third edition). Singapore: McGraw-Hill.
- Bradley, B. A., Jacob, R. W., Hermance, J. F., & Mustard, J. F. (2007). A curve fitting procedure to derive inter-annual phenologies from time series of noisy satellite NDVI data. *Remote Sensing of Environment*, 106(2), 137–145.
- Bradley, B. A., & Mustard, J. F. (2008). Comparison of phenology trends by land cover class: A case study in the Great Basin, USA. *Global Change Biology*, 14(2), 334–346.
- Bretherton, C. S., Smith, C., & Wallace, J. M. (1992). An intercomparison of methods for finding coupled patterns in climate data. *Journal of Climate*, 5(6), 541–560.
- Brown, J. C., Jepson, W. E., Kastens, J. H., Wardlow, B. D., Lomas, J. M., & Price, K. P. (2007). Multitemporal, moderate-spatial-resolution remote sensing of modern agricultural production and land modification in the Brazilian Amazon. *GIScience & Remote Sensing*, 44(2), 117–148.
- Brown, M. E., Pinzon, J. E., Didan, K., Morisette, J. T., & Tucker, C. J. (2006). Evaluation of the consistency of long-term NDVI time series derived from AVHRR, SPOT-Vegetation, SeaWiFS, MODIS, and Landsat ETM+ sensors. *IEEE Transactions on Geoscience and Remote Sensing*, 44(7), 1787–1793.
- Bruzzone, L., Smits, P. C., & Tilton, J. C. (2003). Foreword special issue an analysis of multitemporal remote sensing images. *IEEE Transactions on Geoscience and Remote Sensing*, 41(10), 2419–2420.
- Buermann, W., Anderson, B., Tucker, C. J., Dickinson, R. E., Lucht, W., Potter, C. S., & Myneni, R. B. (2003). Interannual covariability in Northern Hemisphere air temperatures and greenness associated with El Niño-Southern Oscillation and the Arctic Oscillation. *Journal of Geophysical Research*, 108(D13). doi:10.1029/2002JD002630.
- Canisius, F., Turrall, H., & Molden, D. (2007). Fourier analysis of historical NOAA time series data to estimate bimodal agriculture. *International Journal of Remote Sensing*, 28(24), 5503–5522.
- Carlson, T., & Ripley, D. (1997). On the relation between NDVI, fractional vegetation cover, and leaf area index. *Remote Sensing of Environment*, 62(3), 241–252.
- Carrao, H., Goncalves, P., & Caetano, M. (2008). Contribution of multispectral and multitemporal information from MODIS images to land cover classification. *Remote Sensing of Environment*, 112(3), 986–997.
- Carrao, H., Goncalves, P., & Caetano, M. (2010). A nonlinear harmonic model for fitting satellite image time series: Analysis and prediction of land cover dynamics. *IEEE Transactions on Geoscience and Remote Sensing*, 48(4), 1919–1930.
- Castro, C. L., Beltrán-Przekurat, A. B., & Pielke, R. A. (2009). Spatiotemporal variability of precipitation, modeled soil moisture, and vegetation greenness in North America within the recent observational record. *Journal of Hydrometeorology*, 10(6), 1355–1378.
- Chen, J. M., Jonsson, P., Tamura, M., Gu, Z. H., Matsushita, B., & Eklundh, L. (2004). A simple method for reconstructing a high-quality NDVI time-series data set based on the Savitzky-Golay filter. *Remote Sensing of Environment*, 91(3–4), 332–344.
- Cihlar, J., Ly, H., Li, Z. Q., Chen, J., Pokrant, H., & Huang, F. T. (1997). Multitemporal, multichannel AVHRR data sets for land biosphere studies – Artifacts and corrections. *Remote Sensing of Environment*, 60(1), 35–57.
- Cihlar, J., Manak, D., & D'lorio, M. (1994). Evaluation of compositing algorithms for AVHRR data over land. *IEEE Transactions on Geoscience and Remote Sensing*, 32(2), 427–437.
- Cohen, W. B., & Goward, S. N. (2004). Landsat's role in ecological applications of remote sensing. *Bioscience*, 54(6), 535–545.
- Coops, N. C., Wulder, M. A., & Iwanicka, D. (2009). Demonstration of a satellite-based index to monitor habitat at continental-scales. *Ecological Indicators*, 9(5), 948–958.
- Coppin, P., Jonckheere, I., Lambin, E., Nackaerts, K., & Muys, B. (2004). Digital change detection methods in ecosystem monitoring: A review. *International Journal of Remote Sensing*, 25(9), 1565–1596.
- Courault, D., Bsaibes, A., Kpemlie, E., Hadria, R., Hagolle, O., Marloie, O., Hanocq, J.-F., Olioso, A., Bertrand, N., & Desfonds, V. (2008). Assessing the potentialities of FORMOSAT-2 data for water and crop monitoring at small regional scale in South-Eastern France. *Sensors*, 8(5), 3460–3481.
- Dash, J., Jegathan, C., & Atkinson, P. M. (2010). The use of MERIS Terrestrial Chlorophyll Index to study spatio-temporal variation in vegetation phenology over India. *Remote Sensing of Environment*, 114(7), 1388–1402.
- Dash, J., Lankester, T., Hubbard, S., & Curran, P. J. (2008). Signal-to-noise ratio for MTCI and NDVI time series data. In H. Lacoste, & L. Ouwehand (Eds.), *Proceedings of the 2nd MERIS(A)ATSR User Workshop Frascati, Italy*.
- Dash, J., Mathur, A., Foody, G. M., Curran, P. J., Chipman, J. W., & Lillesand, T. M. (2007). Land cover classification using multi-temporal MERIS vegetation indices. *International Journal of Remote Sensing*, 28(6), 1137–1159.
- Davis, A., Marshak, A., Wiscombe, W., & Cahalan, R. (1994). Multifractal characterizations of nonstationarity and intermittency in geophysical fields: Observed, retrieved, or simulated. *Geophysical Research Letters*, 99(D4), 8055–8072.
- de Beurs, K. M., & Henebry, G. M. (2005). A statistical framework for the analysis of long image time series. *International Journal of Remote Sensing*, 26(8), 1551–1573.
- De Fries, R. S., Hansen, M., Townshend, J. R. G., & Sohlberg, R. (1998). Global land cover classifications at 8 km spatial resolution: The use of training data derived from Landsat imagery in decision tree classifiers. *International Journal of Remote Sensing*, 19(16), 3141–3168.
- Defries, R. S., Hansen, M. C., & Townshend, J. R. G. (1995). Global discrimination of land cover types from metrics derived from AVHRR pathfinder data. *Remote Sensing of Environment*, 54(3), 209–222.
- Defries, R. S., & Townshend, J. R. G. (1994). NDVI-derived landcover classifications at a global scale. *International Journal of Remote Sensing*, 15(17), 3567–3586.
- Duchemin, B., Goubier, J., & Courrier, G. (1999). Monitoring phenological key stages and cycle duration of temperate deciduous forest ecosystems with NOAA/AVHRR data. *Remote Sensing of Environment*, 167(1), 68–82.
- Duchemin, B., Hagolle, O., Mougnot, B., Benhadji, I., Hadria, R., Simonneaux, V., Ezzahar, J., Hoedjes, J., Khabba, S., Kharrou, M. H., Boulet, G., Dedieu, G., Er-Raki, S., Escadafal, R., Olioso, A., & Chehbouni, A. G. (2008). Agrometeorological study of semi-arid areas: An experiment for analysing the potential of time series of FORMOSAT-2 images (Tensift-Marrakech plain). *International Journal of Remote Sensing*, 29(17–18), 5291–5300.
- Eastman, J. R., & Fulk, M. (1993). Long sequence time series evaluation using standardized principal components. *Photogrammetric Engineering and Remote Sensing*, 59(8), 1307–1312.
- Ehrlich, D., & Lambin, E. F. (1996). Broad-scale land-cover classification and interannual climatic variability. *International Journal of Remote Sensing*, 17(5), 845–862.
- Eklundh, L., & Olsson, L. (2003). Vegetation index trends for the African Sahel 1982–1999. *Geophysical Research Letters*, 8. doi:10.1029/2002GL016772.
- Evans, J. P., & Geerken, R. (2006). Classifying rangeland vegetation type and coverage using a Fourier component based similarity measure. *Remote Sensing of Environment*, 105(1), 1–8.
- Evrendilek, F., & Gulbeyaz, O. (2008). Deriving vegetation dynamics of natural terrestrial ecosystems from MODIS NDVI/EVI Data over Turkey. *Sensors*, 8(9), 5270–5302.
- Fensholt, R., Nielsen, T. T., & Stisen, S. (2006). Evaluation of AVHRR PAL and GIMMS 10-day composite NDVI time series products using SPOT-4 vegetation data for the African continent. *International Journal of Remote Sensing*, 27(13), 2719–2733.
- Fensholt, R., Sandholt, I., & Rasmussen, M. S. (2004). Evaluation of MODIS LAI, fAPAR and the relation between fAPAR and NDVI in a semi-arid environment using in situ measurements. *Remote Sensing of Environment*, 91(3–4), 480–507.
- Fischlin, A., Midgley, G., Price, J., Leemans, R., Gopal, B., Turley, C., Rounsevell, M., Dube, O., Tarazona, J., & Velichko, A. (2007). Ecosystems, their properties, goods, and services. In M. Parry, O. Canziani, J. Palutikof, P. van der Linden, & C. Hanson (Eds.), *Climate change 2007: Impacts, adaptation and vulnerability. Contribution of Working Group II to the Fourth Assessment Report of the Intergovernmental Panel on Climate Change* (pp. 211–272). Cambridge: Cambridge University Press.
- Foody, G. M. (2002). Status of land cover classification accuracy assessment. *Remote Sensing of Environment*, 80(1), 185–201.
- Fovell, R. G., & Fovell, M. C. (1993). Climate zones of the conterminous United States defined using cluster-analysis. *Journal of Climate*, 6(11), 2103–2135.
- Friedl, M. A., McIver, D. K., Hodges, J. C., Zhang, X. Y., Muchoney, D., Strahler, A. H., Woodcock, C. E., Gopal, S., Schneider, A., Cooper, A., Baccini, A., Gao, F., & Schaaf, C. (2002). Global land cover mapping from MODIS: Algorithms and early results. *Remote Sensing of Environment*, 83(1–2), 287–302.
- Friedl, M. A., Sulla-Menashe, D., Tan, B., Schneider, A., Ramankutty, N., Sibley, A., & Huang, X. (2010). MODIS Collection 5 global land cover: Algorithm refinements and characterization of new datasets. *Remote Sensing of Environment*, 114(1), 168–182.
- Gao, F., Morisette, J. T., Wolfe, R. E., Ederer, G., Pedelty, J., Masuoka, E., Myneni, R., Tan, B., & Nightingale, J. (2008). An algorithm to produce temporally and spatially continuous MODIS-LAI time series. *IEEE Geoscience and Remote Sensing Letters*, 5(1), 60–64.
- Geerken, R., Batikha, N., Celis, D., & Depauw, E. (2005a). Differentiation of rangeland vegetation and assessment of its status: Field investigations and MODIS and SPOT VEGETATION data analyses. *International Journal of Remote Sensing*, 26(20), 4499–4526.
- Geerken, R., Zaitchik, B., & Evans, J. P. (2005b). Classifying rangeland vegetation type and fractional cover of semi-arid and arid vegetation covers from NDVI time-series. *International Journal of Remote Sensing*, 26(24), 5535–5554.
- Glenn, E. P., Huete, A. R., Nagler, P. L., & Nelson, S. G. (2008). Relationship between remotely-sensed vegetation indices, canopy attributes and plant physiological processes: What vegetation indices can and cannot tell us about the landscape. *Sensors*, 8(4), 2136–2160.
- Gong, D. Y., & Ho, C. H. (2003). Detection of large-scale climate signals in spring vegetation index (Normalized Difference Vegetation Index) over the Northern Hemisphere. *Journal of Geophysical Research*, 108(D16, 4498). doi:10.1029/2002JD002300.
- Gong, X., & Richman, M. B. (1995). On the application of cluster-analysis to growing-season precipitation data in North America east of the rockies. *Journal of Climate*, 8(4), 897–931.
- Gong, D. Y., & Shi, P. J. (2003). Northern hemispheric NDVI variations associated with large-scale climate indices in spring. *International Journal of Remote Sensing*, 24(12), 2559–2566.
- Gong, D. Y., & Shi, P. J. (2004). Inter-annual changes in Eurasian continent NDVI and its sensitivity to the large-scale climate variations in the last 20 years. *Acta Botanica Sinica*, 46(2), 186–193.
- Granger, C. W. J., & Newbold, P. (1974). Spurious regressions in econometrics. *Journal of Econometrics*, 2(2), 111–120.
- Gurgel, H. C., & Ferreira, N. J. (2003). Annual and interannual variability of NDVI in Brazil and its connections with climate. *International Journal of Remote Sensing*, 24(18), 3595–3609.
- Hadria, R., Duchemin, B., Jarlan, L., Dedieu, G., Baup, F., Khabba, S., Olioso, A., & Le Toan, T. (2010). Potentiality of optical and radar satellite data at high spatio-temporal resolutions for the monitoring of irrigated wheat crops in Morocco. *International Journal of Applied Earth Observation and Geoinformation*, 12, S32–S37.
- Halkidi, M., Batistakis, Y., & Vazirgiannis, M. (2001). On clustering validation techniques. *Journal of Intelligent Information Systems*, 17(2–3), 107–145.
- Hall-Beyer, M. (2003). Comparison of single-year and multiyear NDVI time series principal components in cold temperate biomes. *IEEE Transactions on Geoscience and Remote Sensing*, 41(11), 2568–2574.

- Hansen, M. C., DeFries, R. S., Townshend, J. R. G., Carroll, M., Dimiceli, C., & Sohlberg, R. A. (2003). Global percent tree cover at a spatial resolution of 500 meters: First results of the MODIS vegetation continuous fields algorithm. *Ecological Interactions*, 7(10), 1–15.
- Hansen, M. C., Defries, R. S., Townshend, J. R. G., & Sohlberg, R. (2000). Global land cover classification at 1 km spatial resolution using a classification tree approach. *International Journal of Remote Sensing*, 21(6–7), 1331–1364.
- Hernance, J. F., Jacob, R. W., Bradley, B. A., & Mustard, J. F. (2007). Extracting phenological signals from multiyear AVHRR NDVI time series: Framework for applying high-order annual splines with roughness damping. *IEEE Transactions on Geoscience and Remote Sensing*, 45(10), 3264–3276.
- Herold, M., Mayaux, P., Woodcock, C. E., Baccini, A., & Schullius, C. (2008). Some challenges in global land cover mapping: An assessment of agreement and accuracy in existing 1 km datasets. *Remote Sensing of Environment*, 112(2), 2538–2556.
- Herrmann, S. M., Anyamba, A., & Tucker, C. J. (2005). Recent trends in vegetation dynamics in the African Sahel and their relationship to climate. *Global Environmental Change*, 15, 394–404.
- Heumann, B. W., Seaquist, J. W., Eklundh, L., & Jonsson, P. (2007). AVHRR derived phenological change in the Sahel and Soudan, Africa, 1982–2005. *Remote Sensing of Environment*, 108(4), 385–392.
- Hill, M. J., & Donald, G. E. (2003). Estimating spatio-temporal patterns of agricultural productivity in fragmented landscapes using AVHRR NDVI time series. *Remote Sensing of Environment*, 84(3), 367–384.
- Hird, J. N., & McDermid, G. J. (2009). Noise reduction of NDVI time series: An empirical comparison of selected techniques. *Remote Sensing of Environment*, 113(1), 248–258.
- Hirosawa, Y., Marsh, S. E., & Kliman, D. H. (1996). Application of standardized principal component analysis to land-cover characterization using multitemporal AVHRR data. *Remote Sensing of Environment*, 58(3), 267–281.
- Holben, B. N. (1986). Characterization of maximum value composites from temporal AVHRR data. *International Journal of Remote Sensing*, 7(11), 1417–1434.
- Hotelling, H. (1933). Analysis of a complex of statistical variables into principal components. *Journal of Educational Psychology*, 24(6), 417–441.
- Huang, S., & Sieger, F. (2006). Land cover classification optimized to detect areas at risk of desertification in North China based on SPOT VEGETATION imagery. *Journal of Arid Environments*, 67(2), 308–327.
- Huemmerich, K. F., Privette, J. L., Mukelabai, M., Myneni, R. B., & Knyazikhin, Y. (2005). Time-series validation of MODIS land biophysical products in a Kalahari woodland, Africa. *International Journal of Remote Sensing*, 26(19), 4381–4398.
- Huete, A., Didan, K., Miura, T., Rodriguez, E. P., Gao, X., & Ferreira, L. G. (2002). Overview of the radiometric and biophysical performance of the MODIS vegetation indices. *Remote Sensing of Environment*, 83(1–2), 195–213.
- Huete, A. R., Liu, H. Q., Batchily, K., & van Leeuwen, W. (1997). A comparison of vegetation indices over a global set of TM images for EOS-MODIS. *Remote Sensing of Environment*, 59(3), 440–451.
- Jackson, J. E. (1991). *A user's guide to principal components*. New York: John Wiley & Sons, Inc.
- Jacquin, A., Sheeren, D., & Lacombe, J.-P. (2010). Vegetation cover degradation assessment in Madagascar savanna based on trend analysis of MODIS NDVI time series. *International Journal of Applied Earth Observation and Geoinformation*, 12, S3–S10.
- Jain, A. K., Murty, M. N., & Flynn, P. J. (1999). Data clustering: A review. *ACM Computing Surveys*, 31(3), 264–323.
- Jakubauskas, M. E., Legates, D. R., & Kastens, J. H. (2002). Crop identification using harmonic analysis of time series AVHRR NDVI data. *Computers and Electronics in Agriculture*, 37(1–3), 127–139.
- Jiang, B., Liang, S., Wang, J., & Xiao, Z. (2010). Modeling MODIS LAI time series using three statistical methods. *Remote Sensing of Environment*, 114(7), 1432–1444.
- Jin, S., & Sader, S. A. (2005). MODIS time-series imagery for forest disturbance detection and quantification of patch size effects. *Remote Sensing of Environment*, 99(4), 462–470.
- Jolliffe, I. T. (2002). *Principal component analysis*. New York: Springer.
- Jönsson, P., & Eklundh, L. (2002). Seasonality extraction by function fitting to time-series of satellite sensor data. *IEEE Transactions on Geoscience and Remote Sensing*, 40(8), 1824–1832.
- Jönsson, P., & Eklundh, L. (2004). TIMESAT – A program for analyzing time-series of satellite sensor data. *Computers and Geosciences*, 30(8), 833–845.
- Ju, J., & Roy, D. P. (2008). The availability of cloud-free Landsat ETM plus data over the conterminous United States and globally. *Remote Sensing of Environment*, 112(3), 1196–1211.
- Ju, J., Roy, D. P., Shuai, Y., & Schaaf, C. (2010). Development of an approach for generation of temporally complete daily nadir MODIS reflectance time series. *Remote Sensing of Environment*, 114(1), 1–20.
- Julien & Sobrino (2008). NDVI seasonal amplitude and its variability. *International Journal of Remote Sensing*, 29(17), 4887–4888.
- Julien, Y., & Sobrino, J. A. (2009). Comparison of cloud-reconstruction methods for time series of composite NDVI data. *Remote Sensing of Environment*, 114(3), 618–625.
- Julien, Y., & Sobrino, J. A. (2009). The Yearly Land Cover Dynamics (YLCD) method: An analysis of global vegetation from NDVI and LST parameters. *Remote Sensing of Environment*, 113(2), 329–334.
- Justice, C., & Hiernaux, P. (1986). Monitoring grasslands of the Sahel using NOAA AVHRR data: Niger 1983. *International Journal of Remote Sensing*, 7(11), 1475–1497.
- Kang, S., Running, S. W., Zhao, M., Kimball, J. S., & Glassy, J. (2005). Improving continuity of MODIS terrestrial photosynthesis products using an interpolation scheme for cloudy pixels. *International Journal of Remote Sensing*, 26(8), 1659–1676.
- Kerr, J., & Ostrovsky, M. (2003). From space to species: Ecological applications for remote sensing. *Trends in Ecology & Evolution*, 18(6), 299–305.
- Knudby, A., Newman, C., Shaghude, Y., & Muhando, C. (2010). Simple and effective monitoring of historic changes in nearshore environments using the free archive of Landsat imagery. *International Journal of Applied Earth Observation and Geoinformation*, 12, S116–S122.
- Lambin, E. F. (1996). Change detection at multiple temporal scales: Seasonal and annual variations in landscape variables. *Photogrammetric Engineering and Remote Sensing*, 62(8), 931–938.
- Lambin, E. F., & Ehrlich, D. (1997). Land-cover changes in sub-Saharan Africa (1982–1991): Application of a change index based on remotely sensed surface temperature and vegetation indices at a continental scale. *Remote Sensing of Environment*, 61(2), 181–200.
- Lambin, E. F., & Strahler, A. H. (1994). Change-vector analysis in multitemporal space – A tool to detect and categorize land-cover change processes using high temporal-resolution satellite data. *Remote Sensing of Environment*, 48(2), 231–244.
- Latifovic, R., Cihlar, J., & Chen, J. (2003). A comparison of BRDF models for the normalization of satellite optical data to a standard sun-target-sensor geometry. *IEEE Transactions on Geoscience and Remote Sensing*, 41(8), 1889–1898.
- Lawrence, R. L., & Ripple, W. J. (1999). Calculating change curves for multitemporal satellite imagery: Mount St. Helens 1980–1995. *Remote Sensing of Environment*, 67(3), 309–319.
- Lhermitte, S., Verbesselt, J., Jonckheere, J., van Aardt, J. A. N., Nackaerts, K., Verstraeten, W. W., & Coppin, P. (2008). Hierarchical image segmentation based on similarity of NDVI time series. *Remote Sensing of Environment*, 112(2), 506–521.
- Lhermitte, S., Verbesselt, J., Verstraeten, W. W., & Coppin, P. (2010). A pixel based regeneration index using time series similarity and spatial context. *Photogrammetric Engineering and Remote Sensing*, 76(6), 673–682.
- Lhermitte, S., Verbesselt, J., Verstraeten, W. W., Veraverbeke, S., & Coppin, P. (2011). Assessing intra-annual vegetation regrowth after fire using the pixel based regeneration index. *ISPRS Journal of Photogrammetry and Remote Sensing*, 66, 17–27.
- Liao, T. (2005). Clustering of time series data – A survey. *Pattern Recognition*, 38(11), 1857–1874.
- Lin, Z. Q., & Brannigan, A. (2003). Advances in the analysis of non-stationary time series: An illustration of cointegration and error correction methods in research on crime and immigration. *Quality and Quantity*, 37(2), 151–168.
- Linderman, M., Rowhani, P., Benz, D., Semeels, S., & Lambin, E. (2005). Land-cover change and vegetation dynamics across Africa. *Journal of Geophysical Research*, 110 (D12104). doi:10.1029/2004JD005521.
- Lloyd, D. (1990). A phenological classification of terrestrial vegetation cover using shortwave vegetation index imagery. *International Journal of Remote Sensing*, 11(12), 2269–2279.
- Lobo, A., & Maisongrande, P. (2008). Searching for trends of change through exploratory data analysis of time series of remotely sensed images of SW Europe and NW Africa. *Int J Remote Sens* (2008) vol. 29 (17) pp. 5237–5245. *International Journal of Remote Sensing*, 29(17–18), 5237–5245.
- Los, S. O., Collatz, G. J., Bounoua, L., Sellers, P. J., & Tucker, C. J. (2001). Global interannual variations in sea surface temperature and land surface vegetation, air temperature, and precipitation. *Journal of Climate*, 14(7), 1535–1549.
- Lotsch, A., Friedl, M. A., Anderson, B. T., & Tucker, C. J. (2003). Coupled vegetation-precipitation variability observed from satellite and climate records. *Geophysical Research Letters*, 30(14). doi:10.1029/2003GL017506.
- Loveland, T. R., Merchant, J. W., Brown, J. F., Ohlen, D. O., Reed, B. C., Olson, P., & Hutchinson, J. (1995). Seasonal land-cover regions of the united states. *Annals of the Association of American Geographers*, 85, 339–355.
- Loveland, T. R., Reed, B. C., Brown, J. F., Ohlen, D. O., Zhu, Z., Yang, L., & Merchant, J. W. (2000). Development of a global land cover characteristics database and IGBP DISCover from 1 km AVHRR data. *International Journal of Remote Sensing*, 21(6–7), 1303–1330.
- Lu, X., Liu, R., Liu, J., & Liang, S. (2007). Removal of noise by wavelet method to generate high quality temporal data of terrestrial MODIS products. *Photogrammetric Engineering and Remote Sensing*, 73(10), 1129–1139.
- Lu, D., Mausel, P., Brondizio, E., & Mora, E. (2003). Change detection techniques. *International Journal of Remote Sensing*, 25(12), 2365–2407.
- Lu, H., Raupach, M. R., McVicar, T. R., & Barrett, D. J. (2003). Decomposition of vegetation cover into woody and herbaceous components using AVHRR NDVI time series. *Remote Sensing of Environment*, 86(1), 1–18.
- Lu, D., & Weng, Q. (2007). A survey of image classification methods and techniques for improving classification performance. *International Journal of Remote Sensing*, 28(5), 823–870.
- Lucht, W., & Lewis, P. (2000). Theoretical noise sensitivity of BRDF and albedo retrieval from the EOS-MODIS and MISR sensors with respect to angular sampling. *International Journal of Remote Sensing*, 21(1), 81–98.
- Ma, M. G., & Veroustraete, F. (2006). Reconstructing Pathfinder AVHRR land NDVI time-series data for the Northwest of China. *Advances in Space Research*, 37(4), 835–840.
- Mahalanobis, P. C. (1936). On the generalized distance in statistics. *Proceedings of the National Institute of Science in India*, 2(1), 49–55.
- Mann, M. E., & Lees, J. M. (1996). Robust estimation of background noise and signal detection in climatic time series. *Climatic Change*, 33(3), 409–445.
- Mantua, N. (2004). Methods for detecting regime shifts in large marine ecosystems: A review with approaches applied to North Pacific data. *Progress in Oceanography*, 60(2–4), 165–182.
- Mas, J. F. (1999). Monitoring land-cover changes: A comparison of change detection techniques. *International Journal of Remote Sensing*, 20(1), 139–152.

- Matricardi, E. A., Skole, D. L., Pedlowski, M. A., Chomentowski, W., & Fernandes, L. C. (2010). Assessment of tropical forest degradation by selective logging and fire using Landsat imagery. *Remote Sensing of Environment*, 114(5), 1117–1129.
- Meek, D. W., Prueger, J. H., Sauer, T. J., Kustas, W. P., Hipps, L. E., & Hatfield, J. L. (1999). A note on recognizing autocorrelation and using autoregression. *Agricultural and Forest Meteorology*, 96(1–3), 9–17.
- Mimmack, G. M., Mason, S. J., & Galpin, J. S. (2001). Choice of distance matrices in cluster analysis: Defining regions. *Journal of Climate*, 14(12), 2790–2797.
- Moody, A., & Johnson, D. M. (2001). Land-surface phenologies from AVHRR using the discrete Fourier transform. *Remote Sensing of Environment*, 75(3), 305–323.
- Myneni, R. B., Keeling, C. D., Tucker, C. J., Asrar, G., & Nemani, R. R. (1997). Increased plant growth in the northern high latitudes from 1981 to 1991. *Nature*, 386(6626), 698–702.
- Nezlin, N. P., Kostianoy, A. G., & Li, B. (2005). Inter-annual variability and interaction of remote-sensed vegetation index and atmospheric precipitation in the Aral Sea region. *Journal of Arid Environments*, 62(4), 677–700.
- Oak Ridge National Laboratory Distributed Active Archive Center (ORNL DAAC) (2010). MODIS subsetted land products, Collection 5. Available on-line. <http://daac.ornl.gov/MODIS/modis.html> from ORNL DAAC, Oak Ridge, Tennessee, U.S.A. Accessed Month 07, 2010
- Olden, J., & Neff, B. (2001). Cross-correlation bias in lag analysis of aquatic time series. *Marine Biology*, 138(5), 1063–1070.
- Olthof, I., Pouliot, D., Latifovic, R., & Chen, W. (2008). Recent (1986–2006) vegetation-specific NDVI trends in Northern Canada from satellite data. *Arctic*, 3(61), 381–394.
- Pearson, K. (1901). On lines and planes of closest fit to systems of points in space. *Philosophical Magazine*, 2(6), 559–572.
- Pettorelli, N., Vik, J., Mysterud, A., Gaillard, J., Tucker, C., & Stenseth, N. (2005). Using the satellite-derived NDVI to assess ecological responses to environmental change. *Trends in Ecology & Evolution*, 20(9), 503–510.
- Potter, C. S., & Brooks, V. (1998). Global analysis of empirical relations between annual climate and seasonality of NDVI. *International Journal of Remote Sensing*, 19(15), 2921–2948.
- Prasad, A. K., Sarkar, S., Singh, R. P., & Kafatos, M. (2007). Inter-annual variability of vegetation cover and rainfall over India. *Advances in Space Research*, 39(1), 79–87.
- Reed, B. C., Brown, J. F., Vanderzee, D., Loveland, T. S., Merchant, J. W., & Ohlen, D. O. (1994). Measuring phenological variability from satellite imagery. *Journal of Vegetation Science*, 5(5), 703–714.
- Ricotta, C., Avena, G., & De Palma, A. (1999). Mapping and monitoring net primary productivity with AVHRR NDVI time-series: Statistical equivalence of cumulative vegetation indices. *ISPRS Journal of Photogrammetry and Remote Sensing*, 54(5–6), 325–331.
- Röder, A., Hill, J., Duguay, B., Alloza, J. A., & Vallejo, R. (2008). Using long time series of Landsat data to monitor fire events and post-fire dynamics and identify driving factors. A case study in the Ayora region (eastern Spain). *Remote Sensing of Environment*, 112(1), 259–273.
- Röder, A., Udelhoven, T., Hill, J., del Barrio, G., & Tsiouris, G. (2008). Trend analysis of Landsat-TM and -ETM+ imagery to monitor grazing impact in a rangeland ecosystem in Northern Greece. *Remote Sensing of Environment*, 112(6), 2863–2875.
- Rodgers, J. L., & Nicewander, W. A. (1988). Thirteen ways to look at the correlation coefficient. *The American Statistician*, 42(1), 59–66.
- Roerink, G. J., Menenti, M., & Verhoef, W. (2000). Reconstructing cloudfree NDVI composites using Fourier analysis of time series. *International Journal of Remote Sensing*, 21(9), 1911–1917.
- Running, S. W., Nemani, R. R., Heinsch, F. A., Zhao, M. S., Reeves, M., & Hashimoto, H. (2004). A continuous satellite-derived measure of global terrestrial primary production. *Bioscience*, 54(6), 547–560.
- Sakamoto, T., Yokozawa, M., Toritani, H., Shibayama, M., Ishitsuka, N., & Ohno, H. (2005). A crop phenology detection method using time-series MODIS data. *Remote Sensing of Environment*, 96(3–4), 366–374.
- Samson, S. A. (1993). Two indices to characterize temporal patterns in the spectral response of vegetation. *Photogrammetric Engineering and Remote Sensing*, 59(4), 511–517.
- Sarkar, S., & Kafatos, M. (2004). Interannual variability of vegetation over the Indian sub-continent and its relation to the different meteorological parameters. *Remote Sensing of Environment*, 90(2), 268–280.
- Seiler, R., Kogan, F., Wei, G., & Vinocur, M. (2007). Seasonal and interannual responses of the vegetation and production of crops in Cordoba, Argentina assessed by AVHRR derived vegetation indices. *Advances in Space Research*, 39(1), 88–94.
- Serneels, S., Linderman, M., & Lambin, E. F. (2007). A multilevel analysis of the impact of land use on interannual land-cover change in East Africa. *Ecosystems*, 10(3), 402–418.
- Simoniello, T., Lanfredi, M., Liberti, M., Coppola, R., & Macchiato, M. (2008). Estimation of vegetation cover resilience from satellite time series. *Hydrology and Earth System Sciences*, 12(4), 1053–1064.
- Simonneau, V., Duchemin, B., Helson, D., Er-Raki, S., Olioso, A., & Chehbouni, A. G. (2008). The use of high-resolution image time series for crop classification and evapotranspiration estimate over an irrigated area in central Morocco. *International Journal of Remote Sensing*, 29(1), 95–116.
- Singh, A. (1989). Digital change detection techniques using remotely-sensed data. *International Journal of Remote Sensing*, 10(6), 989–1003.
- Somers, B., Delalieux, S., Stuckens, J., Verstraeten, W. W., & Coppin, P. (2009). A weighted linear spectral mixture analysis approach to address endmember variability in agricultural production systems. *International Journal of Remote Sensing*, 30(1), 139–147.
- Soria, G., & Sobrino, J. A. (2007). ENVISAT/AATSR derived land surface temperature over a heterogeneous region. *Remote Sensing of Environment*, 111(4), 409–422.
- Soudani, K., le Maire, G., Dufrene, E., Francois, C., Delpierre, N., Ulrich, E., & Cecchini, S. (2008). Evaluation of the onset of green-up in temperate deciduous broadleaf forests derived from Moderate Resolution Imaging Spectroradiometer (MODIS) data. *Remote Sensing of Environment*, 112(5), 2643–2655.
- Strahler, A. H., Boschetti, L., Foody, G. M., Friedl, M. A., Hansen, M. C., Herold, M., Mayaux, P., Morisette, J. T., Stehman, S. V., & Woodcock, C. E. (2006). *Global Land Cover Validation: Recommendations for Evaluation and Accuracy Assessment of Global Land Cover Maps*. GFOC-GOLD Report No. 25. Luxembourg: Office for Official Publications of the European Communities.
- Studer, S., Stöckli, R., Appenzeller, C., & Vidale, P. L. (2007). A comparative study of satellite and ground-based phenology. *International Journal of Biometeorology*, 51(5), 405–414.
- Thenkabail, P. S., Enclona, E. A., Ashton, M. S., Legg, C., & De Dieu, M. J. (2004). Hyperion, IKONOS, ALL, and ETM+ sensors in the study of African rainforests. *Remote Sensing of Environment*, 90(1), 23–43.
- Tippett, M. K., DeSole, T., Mason, S. J., & Barnston, A. G. (2008). Regression-based methods for finding coupled patterns. *Journal of Climate*, 21(17), 4384–4398.
- Tottrup, C., & Rasmussen, M. S. (2004). Mapping long-term changes in savannah crop productivity in Senegal through trend analysis of time series of remote sensing data. *Agriculture, Ecosystems and Environment*, 103(3), 545–560.
- Turner, B. L., Lambin, E., & Reenberg, A. (2007). The emergence of land change science for global environmental change and sustainability. *Proceedings of the National Academy of Sciences of the United States of America*, 104(52), 20666–20671.
- Van der Meer, F., & Bakker, W. (1997). CCSM: Cross correlogram spectral matching. *International Journal of Remote Sensing*, 18(5), 1197–1201.
- Vanacker, V., Linderman, M., Lupo, F., Flasse, S., & Lambin, E. (2005). Impact of short-term rainfall fluctuation on interannual land cover change in sub-Saharan Africa. *Global Ecology and Biogeography*, 14(2), 123–135.
- Vasseur, D. A., & Yodzis, P. (2004). The color of environmental noise. *Ecology*, 85(4), 1146–1152.
- Veraverbeke, S., Lhermitte, S., Verstraeten, W. W., & Goossens, R. (2010). The temporal dimension of differenced Normalized Burn Ratio (dNBR) fire/burn severity studies: The case of the large 2007 Peloponnese wildfires in Greece. *Remote Sensing of Environment*, 114(11), 2548–2563.
- Verbesselt, J., Hyndman, R., Newnham, G., & Culvenor, D. (2010a). Detecting trend and seasonal changes in satellite image time series. *Remote Sensing of Environment*, 114(1), 106–115.
- Verbesselt, J., Hyndman, R., Zeileis, A., & Culvenor, D. (2010b). Phenological change detection while accounting for abrupt and gradual trends in satellite image time series. *Remote Sensing of Environment*, 114(12), 2970–2980.
- Verbesselt, J., Jönsson, P., Lhermitte, S., Jonckheere, I., van Aardt, J., & Coppin, P. (2006). Relating time-series of meteorological and remote sensing indices to monitor vegetation moisture dynamics. In C. Chen (Ed.), *Signal and image processing for remote sensing* (pp. 153–173). University of Massachusetts, North Dartmouth, USA: CRC Press.
- Verbesselt, J., Jönsson, P., Lhermitte, S., van Aardt, J., & Coppin, P. (2006). Evaluating indices derived from satellite and climate data as fire risk indicators in savanna ecosystems. *IEEE Transactions on Geoscience and Remote Sensing*, 44(6), 1622–1632.
- Verbesselt, J., Robinson, A., Stone, C., & Culvenor, D. (2009). Forecasting tree mortality using change metrics derived from MODIS satellite data. *Forest Ecology and Management*, 258(7), 1166–1173.
- Verbesselt, J., Somers, B., Lhermitte, S., Jonckheere, I., van Aardt, J., & Coppin, P. (2007). Monitoring herbaceous fuel moisture content with SPOT VEGETATION time-series for fire risk prediction in savanna ecosystems. *Remote Sensing of Environment*, 108(4), 357–368.
- Vermote, E., Justice, C. O., & Breon, F. -M. (2009). Towards a generalized approach for correction of the BRDF effect in MODIS directional reflectances. *IEEE Transactions on Geoscience and Remote Sensing*, 47(3), 898–908.
- Verstraeten, W. W., Veroustraete, F., Wagner, W., Van Roey, T., Heyns, W., Verbeiren, S., & Feyen, J. (2010). Impact assessment of remotely sensed soil moisture on ecosystem carbon fluxes across Europe. *Climatic Change*, 103, 117–136.
- Viovy, N. (2000). Automatic Classification of Time Series (ACTS): A new clustering method for remote sensing time series. *International Journal of Remote Sensing*, 21(6–7), 1537–1560.
- Viovy, N., Arino, O., & Belward, A. S. (1992). The Best Index Slope Extraction (BISE): A method for reducing noise in NDVI time-series. *International Journal of Remote Sensing*, 13(8), 1585–1590.
- Vogelmann, J. E., & DeFelicis, T. P. (2003). Characterization of intra-annual reflectance properties of land cover classes in southeastern South Dakota using Landsat TM and ETM+ data. *Canadian Journal of Remote Sensing*, 29(2), 219–229.
- Wagenseil, H., & Samimi, C. (2006). Assessing spatio-temporal variations in plant phenology using Fourier analysis on NDVI time series: Results from a dry savannah environment in Namibia. *International Journal of Remote Sensing*, 16(20), 3455–3471.
- Wang, Q., Adiku, S., Tenhunen, J., & Granier, A. (2005). On the relationship of NDVI with leaf area index in a deciduous forest site. *Remote Sensing of Environment*, 94(2), 244–255.
- Wang, L., Chen, J., Gong, P., Shimazaki, H., & Tamura, M. (2009). Land cover change detection with a cross-correlogram spectral matching algorithm. *International Journal of Remote Sensing*, 30(12), 3259–3273.
- Wardlow, B. D., Egbert, S. L., & Kastens, J. H. (2007). Analysis of time-series MODIS 250 m vegetation index data for crop classification in the US Central Great Plains. *Remote Sensing of Environment*, 108(3), 290–310.
- White, M. A., de Beurs, K. M., Didan, K., Inouye, D. W., Richardson, A. D., Jensen, O. P., O'Keefe, J., Zhang, G., Nemani, R. R., van Leeuwen, W. J., Brown, J. F., de Wit, A.,

- Schaepman, M., Lin, X., Dettinger, M., Bailey, A. S., Kimball, J., Schwartz, M. D., Baldocchi, D. D., Lee, J. T., & Lauenroth, W. K. (2009). Intercomparison, interpretation, and assessment of spring phenology in North America estimated from remote sensing for 1982–2006. *Global Change Biology*, *15*(10), 2335–2359.
- White, M. A., Hoffman, F., Hargrove, W. W., & Nemani, R. R. (2005). A global framework for monitoring phenological responses to climate change. *Geophysical Research Letters*, *32*(L04705). doi:10.1029/2004GL021961.
- Xia, Z., Rui, S., Bing, Z., & Qingxi, T. (2008). Land cover classification of the North China Plain using MODIS EVI time series. *ISPRS Journal of Photogrammetry and Remote Sensing*, *63*(4), 476–484.
- Xiang, B., & Liu, J. -Y. (2002). Relationship between land cover and monsoon interannual variations in east Asia. *Journal of Geographic Science*, *12*(1), 42–48.
- Xiao, X., Hagen, S., Zhang, Q., Keller, M., & Moore, B. (2006). Detecting leaf phenology of seasonally moist tropical forests in South America with multi-temporal MODIS images. *Remote Sensing of Environment*, *103*(4), 465–473.
- Yiou, P., Baert, E., & Loutre, M. F. (1996). Spectral analysis of climate data. *Surveys in Geophysics*, *17*(6), 619–663.
- Yule, G. U. (1926). Why do we sometimes get nonsense-correlations between Time-Series? A study in sampling and the nature of time-series. *Journal of the Royal Statistical Society*, *89*(1), 1–63.
- Zhang, X., Friedl, M. A., & Schaaf, C. B. (2006). Global vegetation phenology from Moderate Resolution Imaging Spectroradiometer (MODIS): Evaluation of global patterns and comparison with in situ measurements. *Journal of Geophysical Research*, *111*(G04017). doi:10.1029/2006JG000217.
- Zhang, X., Friedl, M. A., & Schaaf, C. B. (2009). Sensitivity of vegetation phenology detection to the temporal resolution of satellite data. *International Journal of Remote Sensing*, *30*(8), 2061–2074.
- Zhang, X., Friedl, M., Schaaf, C., Strahler, A., Hodges, J., Gao, F., Reed, B., & Huete, A. (2003). Monitoring vegetation phenology using MODIS. *Remote Sensing of Environment*, *84*(3), 471–475.
- Zhang, J., Rivard, B., Sánchez-Azofeifa, A., & Castro-Esau, K. (2006). Intra- and inter-class spectral variability of tropical tree species at La Selva, Costa Rica: Implications for species identification using HYDICE imagery. *Remote Sensing of Environment*, *105*(2), 129–141.
- Zhao, M. S., Heinsch, F. A., Nemani, R. R., & Running, S. W. (2005). Improvements of the MODIS terrestrial gross and net primary production global data set. *Remote Sensing of Environment*, *95*(2), 164–176.
- Zhou, L. M., Tucker, C. J., Kaufmann, R. K., Slayback, D., Shabanov, N. V., & Myneni, R. B. (2001). Variations in northern vegetation activity inferred from satellite data of vegetation index during 1981 to 1999. *Journal of Geophysical Research*, *106*(D17), 20069–20083.
- Zoffoli, M. L., Kandus, P., Madanes, N., & Calvo, D. H. (2008). Seasonal and interannual analysis of wetlands in South America using NOAA-AVHRR NDVI time series: The case of the Parana Delta Region. *Landscape Ecology*, *23*(7), 833–848.
- Zwiers, F. W., & Von Storch, H. (2004). On the role of statistics in climate research. *International Journal of Climatology*, *24*(6), 665–680.